MASTER THESIS
FACULTY OF SCIENCE, UNIVERSITY OF BERN

Fire Signal Detection in Remote Sensing Carbon Data

MARTINA BURGER

Matriculation Number: 16-050-288
Contact: martina.burger@students.unibe.ch

Supervisor: Prof. Dr. Olivia Romppainen-Martius[1]
Co-Supervisor: Prof. Dr. Sonia I. Seneviratne[2]
Advisors: Dr. Lukas Gudmundsson[2] and Verena Bessenbacher[2]

[1] *Oeschger Center for Climate Change Research, University of Bern, Bern, Switzerland*
and
[2] *Institute for Atmospheric and Climate Science, ETH Zürich, Zurich, Switzerland*

UNIVERSITÄT BERN

OESCHGER CENTRE
CLIMATE CHANGE RESEARCH

ETH zürich

9th January 2023

Abstract

Land ecosystems take up about one third of anthropogenic CO_2 emissions and slow down the accumulation of carbon in the atmosphere. The atmospheric CO_2 growth rate exhibits large interannual variability, mainly caused by fluctuations in the carbon sequestration of terrestrial ecosystems. Biomass burning contributes substantially to these fluctuations. However, the quantification of fire CO_2 emissions presents a challenge. Here I show that the potential of space-borne CO_2 and CO observations for the study of fires and their impact on the carbon cycle is restricted by insufficient data availability. The carbon data is tested for a fire signal on global to local scales. The carbon and other variables' behaviour over time in relation to fires is studied with time series and event compositing. Furthermore, a novel approach is applied to correct CO_2 data for emissions from other sources, in order to enhance the fire signal in burned area-carbon correlations. A fire signal is detectable in all carbon data; it is dependent on the analysis method, the size of the area inspected, and the vegetation class burned. These controls affect CO_2 and CO data differently. My results emphasise the need for more precise and temporally higher resolved satellite CO_2 observations to further investigate fire CO_2 emissions and foster our understanding of fire-carbon cycle interactions.

Table of Contents

List of Figures

List of Tables

1 Introduction

In recent years, fires have emerged as a central element of global carbon budget variability. Though an integral component for function and biodiversity of many natural habitats, fires adversely impact the Earth system including the climate in a number of ways. They modify vegetation occurrence, type, and species, and thus land surface properties, such as albedo and evapotranspiration (Randerson et al. 2006). Fires not only influence the climate directly through biogeophysical effects (Archibald et al. 2018), but also indirectly via the carbon cycle. According to vegetation models, combustion of biomass globally reduced the terrestrial carbon storage by 10% in the period from 2001 to 2012, while regionally, the reduction could rise to 20%. Moreover, fires lead to emissions of various trace gases and aerosols (Ward et al. 2012). For both reasons—the reduction of the terrestrial carbon sink as well as the direct release of greenhouse gases—fires are one of the primary causes of interannual variability (IAV) in the atmospheric growth rates of, among others, CO_2 and CH_4 (Langenfelds et al. 2002). The IAV in atmospheric CO_2 thus depends to a large degree on the IAV of the terrestrial carbon sink, which is considerably less well-constrained than the ocean carbon sink (Ciais et al. 2013). The tight coupling of the carbon stock's partitioning into land and atmosphere is evident from Fig. 1.

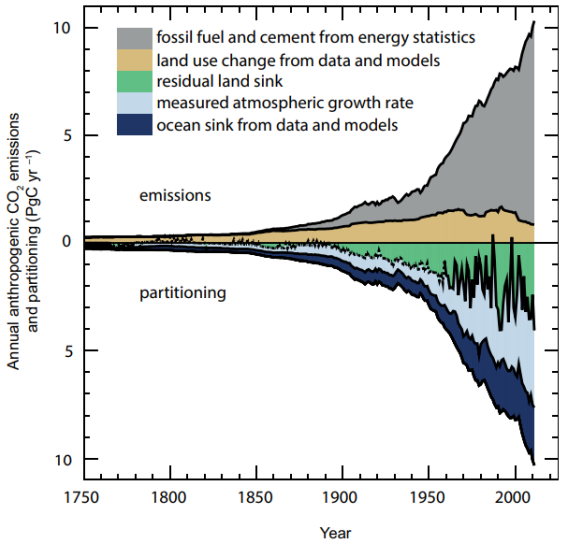

Figure 1: CO_2 sources and sinks (Ciais et al. 2013, IPCC AR5).

In the context of terrestrial and atmospheric carbon stocks, climate change mitigation measures should not go unmentioned. Carbon storage in forests is a key component in the mitigation strategy (Grassi et al. 2017), and it requires thorough understanding of the interaction between fire, vegetation and the carbon cycle. Besides, it is precisely

these interactions, specifically between fire, peatlands, and permafrost thaw, and their response to further warming, which are not yet sufficiently included in climate and Earth system models (Lasslop et al. 2019; IPCC 2021). Fires thus substantially influence the partitioning of carbon into terrestrial and atmospheric pools, which is why it is so important to assess their annual magnitude and impact. In the following subsections the role of fires in the Earth system shall be considered in more detail.

1.1 Literature Review

1.1.1 Fire Ecology

There is an great diversity of fire regimes on Earth. Typical fire characteristics, such as intensity, frequency, extent, and type, as well as their ecosystem impacts, vary considerably over space and time (McLauchlan et al. 2020). The body of scientific literature on fire ecology reflects a paradigm shift from the concept of fire as destructive force to the concept of fire as essential process shaping most ecosystems on land (e.g. Archibald et al. 2018; Bond et al. 2004; He et al. 2018; Pausas et al. 2017; Werf et al. 2006). The net effect of fires on the atmospheric carbon pool depends on the balance of emissions during biomass combustion and the uptake during the vegetation recovery phase (Lasslop et al. 2019). Not all fires are wildfires; many are planned by humans as a means to manage the land. These fires have the same impact on the carbon cycle, however, it can be expected that the global area burned by prescribed fires does not vary dramatically over the years.

The effects of fire on the vegetation depends on a number of factors, such as the fire size, pre- and post-fire climate, plant life-history traits, and recent fire history (Davis et al. 2018; Johnstone et al. 2016). The plant species composition can be perpetuated when dominant species resprout from sheltered basal meristems (Keeley et al. 2005). This applies for example to fires in grasslands, savannas, and many Mediterranean shrublands. By contrast, the post-fire succession in forests is difficult to anticipate, as not only fire severity and plant adaptations influence this process, but also landscape fragmentation, herbivory, interacting disturbances and many more elements (Batllori et al. 2018; Blackhall et al. 2017; Pausas 2015). Particularly in forests, there might be long-term fire consequences. Forests may continue to be net carbon sources ten years after a severe fire, and the transition to grass- or shrubland is possible (Hurteau et al. 2011). Fires do not only change above-ground biomass, but with it also the soil properties. Pyrolysis and combustion reactions destroy the uppermost organic horizon and

the underlying mineral soil might be impacted by conductive and advective heating. In addition to soil organic matter composition, fires can also change the soil structure, composition and activity rates of soil biota, and carbon and nutrient pools and fluxes (Adkins et al. 2019; Gutknecht et al. 2010; Miesel et al. 2015). Overall, individual fire impacts on ecosystems can be almost as diverse as the Earth's ecosystems themselves.

1.1.2 The Interplay of Weather, Climate, and Fire

Above the impacts of fires on the vegetation are described; yet vegetation is not only affected by fires, but in its role as fuel it is also an important driver of fire activity. Fire is the consequence of three co-occurring factors: a stock of fuel, fire weather conditions, and an ignition source, which may be anthropogenic or natural (Bistinas et al. 2014; Forkel et al. 2017; Kelley et al. 2019). Fire weather is a term for meteorological conditions conducive to the ignition and spread of wildfires (Jones et al. 2022). There are numerous indices for fire weather which aim to quantify the flammability (i.e. the dryness) of the vegetation (Jolly et al. 2015) due to combined effects of temperature, precipitation, humidity, and wind (Field et al. 2015). Hot, dry, less humid, and windy conditions prime vegetation to burn. According to the Intergovernmental Panel on Climate Change (IPCC), several climate trends might promote the increasing frequency and intensity of fire weather (Fischer et al. 2021; Jia et al. 2019). Jones et al. (2022) indeed found increases in the length of the fire weather season and the frequency of extreme fire weather during 1979-2019 in most regions globally, which paves the way for more frequent burning of the landscapes.

Climate change, in turn, is perpetuated by global fire activity. Harrison et al. (2018) estimate that fires and related processes cause a rise in atmospheric CO_2 levels of 6 ppm per degree warming of the global mean annual surface temperature. Additionally to this positive feedback, fires are also involved in negative feedback loops. How exactly fire-induced biophysical modifications affect the climate depends on the region and on the time scale inspected (Liu et al. 2019). In high latitudes, forest fires initially cause a warming due to reduced evaporative cooling. Five years after the fire, however, increases in the surface albedo start to predominate the Earth's radiative budget and lead to a net cooling effect. In tropical regions, fires have a slight warming effect because of decreased evapotranspiration. On the global scale, the negative feedbacks only partially offset the positive feedbacks (Jones et al. 2022). Moreover, Saha et al. (2017) suggest that the post-fire surface brightening is responsible for reduced convective precipitation. The interplay of weather, climate, and fire is manifold and highly

complex, and it remains challenging to implement it in Earth system models.

1.1.3 Current Fire Emission Estimates

It is essential to determine the land-atmosphere carbon fluxes as accurately as possible in order to gain a better understanding of the terrestrial carbon sinks. Regional and global CO_2 emissions from fires have been successfully estimated by harnessing the relationship of fire radiative power to biomass burned and (landcover-specific) emission factors (e.g. Pereira et al. 2009; Kaiser et al. 2012). Prominent global fire emission inventories are the Global Fire Emissions Database (GFED, Randerson et al. 2018)), the Global Fire Assimilation System (GFAS, Kaiser et al. 2012)), the Fire Inventory from the National Center for Atmospheric Research (FINN, Wiedinmyer et al. 2011), the Quick Fire Emissions Dataset (QFED, Darmenov et al. 2013), and the Fire Energetics and Emissions Research (FEER, Ichoku et al. 2014). While these data sets have made great contributions in the field of wildfire emission research, they are all based on biomass burning models or on other biogeochemical models, which require remote sensing data input and empirically derived conversion factors (Liu et al. 2020). CO_2 emission estimates strongly depend on such input parameters, each introducing additional uncertainty. Liu et al. (2020) name five major sources of uncertainty in the inventories: 1) primary reliance on accurate active fire and burned area detection, 2) impaired fire detection due to cloud/haze obscuring satellite measurements, 3) fragmentation of burned area, 4) topography roughness, and 5) small fires, which remain undetected. Consequently, model-based fire CO_2 estimates can differ up to 60%, as Shiraishi et al. (2021) show.

Constraining fire CO_2 estimates by satellite observations offers a possible alternative to model estimates. In 2015 and 2016, droughts associated with a pronounced El Niño event occurred widely and contributed to intense fire periods across the globe (Burton et al. 2020). This circumstance triggered the publication of various articles that address the topic of local, regional, and global carbon cycle responses to such events using the same remotely sensed CO_2 product (OCO-2 XCO_2). For example, Heymann et al. (2017) found that the space-based estimate of Indonesian fire CO_2 emissions was about 30% lower than estimates provided by the emission inventories. Guo et al. (2019) identified and characterised smoke plumes of four active wildfires which occurred in Siberia in 2015 using MODIS band 8, band 21 and Multi-angle Imaging Spectroradiometer data. A linear regression model was applied to compute CO_2 for each smoke plume pixel and subsequently, emissions for each wildfire point were calculated. A broader perspect-

ive on carbon cycle responses to the 2015-2016 El Niño event is provided by Crowell et al. (2019), who employed CO_2 data, a large ensemble of atmospheric inversion models, data assimilation methods, and prior flux distributions to confine the total and terrestrial carbon sinks for the years 2015-2016: they found that in situ observations and satellite retrievals constrained similar sinks at global scale, but this agreement decreased when individual regions were inspected. Liu et al. (2017) quantified the reactions of tropical net biosphere carbon exchange, gross primary production, biomass burning, and respiration by assimilating CO_2, solar-induced chlorophyll fluorescence, and carbon monoxide observations from multiple satellites. They conclude that there is no single dominant process determining carbon cycle IAV. In general, previous research on terrestrial carbon sources in relation to El Niño events demonstrates that space-borne derivation of CO_2 emissions on different spatial scales is possible.

A few more case studies have examined the suitability of remote sensing carbon data to determine local or regional fire CO_2 emissions. Guo et al. (2017) identified and characterised smoke plumes of severe Russian wildfires in 2010 by inspecting Cloud and Aerosol Imager retrievals and thermal infrared data. CO_2 changes were derived from shortwave infrared measurements. The resulting CO_2 emission estimate was only slightly lower than the CO_2 emission as estimated by a biomass burning model. Li et al. (2019) inspected satellite monthly mean CO_2 data for the region of California and came to the conclusion that CO_2 increased by 2 ppm after the wildfire in October 2017. Wang et al. (2020) analysed CO_2 data from the same satellite and found that the 2020 Australian mega-bushfires enhanced CO_2 at the outer fringe of smoke plumes by approximately 1.5 ppm. This result was validated using an atmospheric transport model forced by GFED, version 4.1. They concluded that wildfire-induced maximum CO_2 enhancements are detectable to some extent; however, it remains a challenging task due to gaps in the CO_2 retrievals obscured by smoke. van der Velde et al. (2021) also recognised the need for research on fire CO_2 emissions in the case of the exceptional Australian wildfire event in 2019-2020, as prominent fire inventory estimates differ by up to a factor of four for this incident. They constrained CO_2 emission estimates with the help of remotely sensed carbon monoxide, an analytical Bayesian inversion, and observed ratios between CO_2 and CO emissions. They consider CO observations more appropriate for CO_2 emission estimates, as CO values show a much larger relative deviation from background concentrations upon fire events than CO_2 values. The emission estimate derived for November 2019 to January 2020 was verified using a bottom-up bootstrap analysis. It was more than twice as large as the average of five fire inventories.

1.2 Research Questions

Our understanding of wildfire-climate relationships on the large scale remains limited (Tang et al. 2021). Global emission inventories exhibit large inconsistencies in their estimates of fire-induced CO_2 emissions. Instead of a model-derived bottom-up approach, it would thus be highly interesting to find an alternative top-down approach based on satellite observations to generate and compare fire CO_2 emission estimates. Previous scientific work has proven that it is feasible to infer fire CO_2 emission estimates from space-based measurements on different spatial scales, but it involved considerable effort, e.g. using elaborate data assimilation methods or atmospheric inversion models. Few studies have been conducted on global fire CO_2 emissions using remote sensing techniques.

Several CO_2 observing satellite missions with global coverage are currently operating. It is their explicit purpose to collect CO_2 measurements *"with the precision, resolution, and coverage needed to improve our understanding of surface CO_2 sources and sinks (fluxes) on regional scales ($\geq 1000 km$) and the processes controlling their variability over the seasonal cycle"* (NASA 2022). More precisely, NASA states that their carbon observing mission contributes, among others, to studies on *"the exchange of carbon between the atmosphere and tropical ecosystems due to plant growth, respiration, and fires.* ESA formulates similar carbon mission objectives; they emphasise the importance of atmospheric CO_2 monitoring and the research of the global distribution and temporal variation of greenhouse gases on a sub-continental scale (ESA 2022).

With this Master thesis I aim to test the suitability of such satellite-based atmospheric CO_2 and CO observations (summarised as "carbon" data or variables) for carbon cycle studies on different spatial scales. Specifically, my project is intended to broaden the understanding of interactions between fires and the carbon cycle, which is essential to determining the carbon budget remaining to comply with the 2015 Paris Agreement and limit global warming to well below 2°C. A further objective is to evaluate whether these data can be used as a basis for estimating global fire emissions. Thus, the focus of this work lies on analysing the carbon data sets in an exploratory fashion.

The exploration is guided by the following research questions:

1. Is it possible to detect a fire signal in remote sensing carbon data?
2. What is the co-evolution of fire-related variables and burned area data? Could any systematic behaviour of auxiliary variables help to infer CO_2 and CO values where they are missing?

In the context of carbon data, I define "fire signal" as a likely fire-induced enhancement of atmospheric carbon concentrations. In the case of auxiliary variables, a "fire signal" or "fire response" is deemed to exist if they demonstrate anomalies which might be expected in connection with fires.

2 Data

In this and the following subsection I describe the data that build the base of this thesis and the data pre-processing steps. For a quick overview of the data sets and their original properties see Table 1.

2.1 Data Sets

The central parameters for my work are satellite-based observations, most importantly CO_2 and CO data. Further important parameters include burned area (BA), aerosol optical depth (AOD), and land surface temperature (LST). These are closely linked to wildfires and are commonly used to identify fire locations (Csiszar et al. 2006; Wooster et al. 2012; Reid et al. 2012, e.g.). I will henceforth call these primary auxiliary variables. The primary auxiliary variables are extended by secondary auxiliary variables, which are likely to be influenced by fires—or themselves influence fires, e.g. in their build-up—, but the interlinkage is less evident. Secondary auxiliary variables are terrestrial water storage (TWS) and normalised difference vegetation index (NDVI). An additional vegetation index is introduced: the vegetation optical depth at L-band frequency (L-VOD). Furthermore, output data from Dynamic Global Vegetation Models (DGVM) are included in the second part of my analysis, more precisely the parameter Net Biospheric Production (NBP). I preliminarily investigate the introduction of data on anthropogenic carbon emissions. But since they cover only a short time span from 2019 to 2020, and in addition, this time period cannot be deemed representative in

terms of anthropogenic CO_2 emissions due to the COVID-19 pandemic, these data are not considered for the final results.

Table 1: Overview of the data sets for the analyses, indicating the original properties of the products.

Data set	**Variable**	**Temp. cov.**	**Temp. res.**	**Spatial res.**
Multi-Instrument Fused bias-corrected XCO_2	XCO_2	2014-2020	daily	1°
AIRS3STM	CO	2002-2022	monthly	1°
ESA FireCCI51	total BA	2001-2020	monthly	0.25°
ESA FireCCI51	BA in vegetation class	2001-2020	monthly	0.25°
CERES SYN1deg	AOD	2000-2021	monthly	1°
MYD11C1v006	LST	2002-2021	daily	0.05°
GRACE Tellus JPL-RL06M.MSCNv02	TWS	2002-2022	monthly	0.5°
MOD13C2v061	NDVI	2000-2021	monthly	0.05°
SMOS-ICv2	L-VOD	2010-2021	daily	25 km
TRENDY	NBP	1700-2020	monthly	NA*
GRACED**	anthr. C emissions	2019-2020	daily	0.1°

* TRENDY data include a set of DGVM simulations over the historical period, where the individual DGVM simulations differ in spatial resolution.
** GRACED data are experimentally used in the course of the correlation analysis, but they are not part of the final analysis.

Carbon dioxide (CO_2) data for this study are represented by the Multi-Instrument Fused bias-corrected XCO_2 Version 3 product in ppm. As the name says, this is a merged product of column-averaged dry air mole fraction of CO_2 (XCO_2). It was created by applying local kriging to daily aggregates of Orbiting Carbon Observatory (OCO-2) and Greenhouse Gases Observing Satellite (GOSAT) bias-orrected data (Nguyen et al. 2022). The product is gridded at a resolution of $1^\circ \times 1^\circ$ and covers a time span of September 2014 - July 2020. OCO-2 is a polar sun-synchronous orbit satellite with a return cycle of 16 days. It covers a 1.29×2.25 km footprint at nadir and has been operated by the US National Aeronautics and Space Administration (NASA) since July 2014. The imaging spectrometer aboard the OCO-2 measures radiances in the short-wavelength infrared spectral region (0.765 µm, 1.61µ̃m, 2.06 µm) (Worden et al. 2017). Radiative transfer and XCO_2 retrieval algorithms, described e.g. by O'Dell et al. (2012) and Connor et al.

(2008), yield estimations of column-averaged atmospheric CO_2 concentrations. JAXA, the Japan Aerospace Exploration Agency, launched GOSAT in January 2009 (Janardanan et al. 2016). It is also a sun-synchronous satellite, with a repeat cycle of three days and a footprint of approximately 10 km. GOSAT carries the Thermal and Near-infrared Sensor for Carbon Observation-Fourier Transform Spectrometer (TANSO-FTS), with three bands in the short-wavelength infrared region (0.76 µm, 1.6 µm, 2.0 µm) and one broad thermal infrared band between 5.6 and 14.3 µm (Inoue et al. 2013). Yoshida et al. (2011) describe the retrieval algorithm applied to obtain GOSAT XCO_2 estimates. For my analysis, I choose the merged product to ensure the best possible spatial and temporal data coverage. Yet there is a period of 50 days with missing data, from 31 July 2017 to 19 September 2017. For the sake of simplicity, XCO_2 is henceforward only referred to as CO_2. CO_2 enhancements are indicated in ppm, while CO_2 emissions are converted to Gt carbon using the conversion of Friedlingstein et al. (2021) where 1 Gt carbon = 3.664 Gt CO_2.

Carbon monoxide (CO) data are retrieved as mixing ratios from the Atmospheric InfraRed Sounder (AIRS) on the European Space Agency's (ESA's) satellite Aqua. The CO spectral feature is centred around 4.7 µm (Pagano et al. 2022). CO data are available at 24 atmospheric standard pressure levels from 1000 to 1 hPa (Tian et al. 2020). Sensitivity to variations in CO peaks in the mid-troposphere, around 500 hPa (Pagano et al. 2022). The data sets have 1° spatial and monthly temporal resolution and span a period from 2002 to 2022 (AIRS project 2019).

The **Burned Area (BA)** data I use were developed in the ESA Climate Change Initiative programme on the global monitoring of Essential Climate Variables (ECV), since fire disturbance is deemed one of these ECVs (Pettinari et al. 2020). The data set (v5.1) contains 14 variables of which I use two, namely total burned area and burned area in vegetation class, both given in units of m^2. The data set is available as grid product at 0.25° spatial resolution and at a monthly temporal resolution, and covers a period from 2001 to 2020. It is derived from the Moderate Resolution Imaging Spectroradiometer (MODIS) onboard the TERRA satellite. The detection algorithm is based on a hybrid approach, using both thermal anomalies information and near-infrared reflectance values of MODIS (Lizundia-Loiola et al. 2020). 18 vegetation classes are extracted from the Land Cover Climate Change Initiative (LC-CCI) product to assess BA per vegetation class. This product offers annual land cover files covering the period 1992 to 2020. For each year, previous year information was used, except for 2017 to 2020, where the last available year (2015) was used (ESA 2017, LC_CCI v2.0.7). Here I use 17 of the 18 vegetation classes, as there is no occurrence of BA in vegetation class 140 ("lichens and

mosses") in the inspected regions. For details on the vegetation classes, see Pettinari et al. (2020, p. 22).

Biomass burning is an important source of aerosols, it releases primarily black and brown carbon as well as organic aerosols into the atmosphere (Cheng et al. 2013). **Aerosol Optical Depth (AOD)** is a common satellite-based measure to estimate atmospheric aerosol loading; it is a dimensionless measure of the extinction of light (Shinozuka et al. 2007). In this study, the synoptic 1° (SYN1deg) AOD product is used, which was developed in the Clouds and Earth's Radiant Energy System (CERES) project from NASA. AOD is derived from observations of MODIS (on the Aqua and Terra satellites) and its successor (on the Suomi National Polar-orbiting Partnership satellite), the Visible Infrared Imager Radiometer Suite, at the spectral region around 0.55 µm. It is assimilated by an aerosol transport model and covers a period from 2000 to 2021 (Fillmore et al. 2022). The spatial resolution is 1° and the temporal resolution is monthly.

A MODIS **Land Surface Temperature (LST)** product is used, specifically the MYD11C1v006 product from the Aqua satellite. It is created applying a generalised split-window algorithm described by Li et al. (2020a), with MODIS surface emissivity bands 31 (around 11.03 µm) and 32 (12.02 µm). LST data in Kelvin are available at daily time steps with a spatial resolution of 0.05° for the period 2002 - 2021.

Terrestrial Water Storage (TWS), including groundwater, soil moisture, surface waters, snow, and water stored in the biosphere, can be retrieved from microwave measurements. The Gravity Recovery and Climate Experiment (GRACE) mission was established in the early 2000s, as a joint venture between NASA and the Deutsches Zentrum für Luft- und Raumfahrt. The mission consisted of two identical satellites in identical orbits, approximately 220 km apart (Humphrey et al. 2018). The satellites continuously monitor their exact separation distance and its rate versus time, which varies as the satellites pass through changing gravity (Ramillien et al. 2008). The separation distance is determined with the help of a K-Band microwave ranging system. Moreover, the satellites carry Global Positioning System (GPS) receivers and high precision accelerometers, the latter to ensure that only accelerations caused by gravity are considered (Tapley et al. 2004). In combination, these observations allow to derive the changes in water masses on Earth. GRACE yielded TWS data for a period spanning 2002 - 2017, a successor, the GRACE Follow-On (GRACE-FO) was launched in 2018. Together, they cover the period from 2002 to 2022, for which approximately monthly TWS data with 0.5° spatial resolution are available. The data were processed at NASA's Jet Propulsion Laboratory (JPL) to liquid water equivalent height anomalies in cm (Wiese et al. 2016;

Landerer et al. 2020), relative to a time-mean baseline from 2004 to 2009 (Moghim 2020). I use the GRACE Tellus product from release 6, version 2 (Wiese et al. 2019, JPL-RL06M.MSCNv02), which was produced applying the mass concentration (mascon) solution approach. For a detailed description of this approach please refer to Watkins et al. (2015). There are quite a few gaps in the GRACE data set for the relevant time period. On the one hand, single monthly values are missing (Dec 2014, May, June, Oct, and Nov 2015, Apr, Sept, and Oct 2016, Feb 2017, Aug and Sept 2018), on the other hand, there is an entire year of missing data from June 2017 to June 2018.

Normalised Difference Vegetation Index (NDVI) data were collected from MODIS on Terra and used as proxy for vegetation productivity, or plant health. The NDVI is often used to monitor live green vegetation and can be derived from the red to near-infrared reflectance ratio. NDVI values range from -1 to +1, where negative values indicate the absence of vegetation (Pettorelli et al. 2005). The MOD13Cv061 product I use is available at monthly temporal and 0.05° spatial resolution. It covers the period from 2000 to 2021.

As additional vegetation index, I introduce **Vegetation Optical Depth at L-band frequency (L-VOD)** in my analysis as proxy for above-ground biomass. L-VOD is related to the intensity of microwave extinction within the canopy layer and can be derived from active or passive microwave systems. It is only marginally impacted by adverse atmospheric effects, and thus increasingly applied for large-scale ecological studies (Li et al. 2021). The data for this thesis is collected by passive microwave instruments on ESA's Soil Moisture and Ocean Salinity (SMOS) mission, and processed with an algorithm developed by the French Institut National de la Recherche Agronomique and Centre d'Études Spatiales de la Biosphère (Fernandez-Moran et al. 2017; Li et al. 2020a; Li et al. 2020b). I use version 2 of the resulting product, called SMOS-IC v2. Wigneron et al. (2021) have found L-VOD to be a key index to evaluate the inter-annual variations in the above-ground biomass stocks. L-VOD data are in 25 km spatial resolution at daily time steps, and they cover a time span from 2010 to 2021. Values range between 0 and 2, and are of dimensionless unit. There is one day of missing data for the relevant time span, namely 15 March 2016.

Net Biospheric Production (NBP) data is collected from the TRENDY project and serves as estimate of the terrestrial carbon sink. A consortium of DGVM groups set up this project to investigate the spatial trends in NBP and agreed to perform DGVM simulations over the historical period every year since 2010 (Sitch et al. 2015). TRENDY data support the the Global Carbon Project's annual global carbon budget assessments, the

most recent TRENDYv10 data used here are available online for spin-off studies. A total of 17 DGVMs participate in TRENDYv10, the single models and related sources for a detailed description of them can be found in Friedlingstein et al. (2021). In summary, the DGVMs' forcing data include time-dependent gridded climate forcing, global atmospheric CO_2, gridded land cover changes, and some also gridded nitrogen deposition and fertilisers. Four simulations (S0, S1, S2, S3) are performed with each DGVM. Here I use output from S3, which is deemed the most realistic of the four. It applies historical changes in atmospheric CO_2 concentrations, nitrogen inputs, climate, land cover distribution, and wood harvest rates. NBP is the difference of the modelled parameters Net Primary Production (NPP) minus heterotrophic Respiration (Rh). NBP values are in units of kgC m^{-2} s^{-1} at monthly time steps and cover the period 1700 - 2020. The individual DGVMs have different spatial resolution.

A new data set on **anthropogenic CO_2 emissions**, the Global Gridded Daily CO_2 Emissions Dataset (GRACED) was published in November 2021 (Dou et al. 2021). It contains anthropogenic fossil fuel and cement CO_2 emissions in units of KgC d^{-1} for the years 2019 - 2021. It is provided with a spatial resolution of 0.1° and daily temporal resolution. However, the data set I gained access to upon request was in hourly resolution, representing mean hourly values for one day. The emissions are computed based on the national CO_2 emissions data set (Carbon Monitor), the spatial patterns of a point source emission data set (Global Energy Infrastructure Emissions Database), the emission database for global atmospheric research, and spatio-temporal patterns of satellite NO_2 retrievals.

2.2 Data Selection and Preprocessing

There are certain requirements that all data sets must meet. In this Master thesis, data is investigated at different spatial scales, ranging from global to regional. Global data coverage is thus one necessary condition that all data sets must fulfil. Another compelling requirement arises from the temporal extent of the carbon data on which the analyses are based. The period covered by both, CO_2 and CO data, is September 2014 - (and including) July 2020. Accordingly, this is the relevant period that must be covered by all data sets. Furthermore, there is a lower bound for the temporal resolution; data must be available at least once per month. For the spatial resolution there is an upper bound; the spatial resolution can only be moderate to avoid excessive computational costs. Finally, each value needs to be related to three coordinates: latitude, longitude, and time.

2.2.1 The Behaviour of Carbon and Auxiliary Variables in Relation to Fires

There is a number of data preparation steps for this first analysis, some of which apply for all data sets, others are specific to individual data sets. The format I choose for adequate data representation is network common data form (netCDF). Most data sets are available in netCDF, four data sets (CO_2, LST, NDVI, CO) are converted from hierarchical data format to netCDF. The time information is extracted from the file name and added to the data set as coordinate for LST, NDVI, L-VOD, and CO. I sum CO values across all standard pressure levels instead of focusing on CO at one specific altitude, in order to avoid non-observance of CO variation caused by fires, and to make them comparable to CO_2 data, which are also column-averaged. L-VOD also requires additional preparation steps: quality control is executed according to the developers' advice (personal mail correspondence, 13 Jan 2022). Firstly, scene flag values are used to remove L-VOD values impacted by strong topography, frozen, and polluted scenes. Secondly, root mean squared error values between measured and modelled brightness temperature are used to remove L-VOD values strongly impacted by radio frequency interference. Lastly, negative L-VOD values are set to zero, as they are not physically possible. Monthly means are calculated for CO_2, LST, and L-VOD. All data sets are regridded to match the spatial resolution of the BA data set (0.25°). Data exhibiting a noticeable trend are detrended (CO_2, LST, TWS, CO) and seasonality is removed for all data sets by subtracting the mean seasonal cycle. Finally, a land mask is applied for CO_2, AOD, TWS, NDVI, L-VOD, and CO data.

2.2.2 Vegetation-dependent Fire Imprint in different Carbon Data

For the correlation analysis, the relevant parameters are CO_2, CO, BA in vegetation class, and the collection of NBP variables from TRENDY. Here I include TRENDY DGVM runs without active fire modules, as the fire signal is what we would like to emphasise in the carbon data. For one DGVM (DLEM), output data is available only with annual resolution, whereas the temporal resolution for my analysis should be monthly. This yields a set of seven suitable DGVMs (IBIS, ISAM, ORCHIDEEv3, CABLE-POP, OCN, JULES-ES-1.1, YIBs). I convert NBP in kgC m^{-2} s^{-1} to an absolute value in GtC per month. As mentioned above, anthropogenic carbon emissions (GRACED) are introduced tentatively. GRACED data are also converted from mean kgC h^{-1} to GtC per month. For the inspection of BA in vegetation class, I group the 17 land cover categories into seven superordinate vegetation classes (see Table 2).

Table 2: Overview of the grouped vegetation classes.

Vegetation class	**Original land cover category (LC-CCI product)**
Sparse vegetation	Sparse vegetation (tree, shrub, herbaceous cover)(<15%);
Grass	Grassland;
Crop	Cropland, rainfed;
	Cropland, irrigated or post-flooding;
	Mosaic cropland (>50%) / natural vegetation (tree, shrub, herbaceous cover) (<50%);
	Mosaic natural vegetation (tree, shrub, herbaceous cover) (>50%) / cropland (<50%);
Shrub	Shrubland;
	Mosaic tree and shrub (>50%) / herbaceous cover (<50%);
	Mosaic herbaceous cover (>50%) / tree and shrub (<50%);
Tree deciduous	Tree cover, broadleaved, deciduous, closed to open (>15%);
	Tree cover, needleleaved, deciduous, closed to open (>15%);
	Tree cover, mixed leaf type (broadleaved and needleleaved);
Tree evergreen	Tree cover, broadleaved, evergreen, closed to open (>15%);
	Tree cover, needleleaved, evergreen, closed to open (>15%);
Vegetation flooded	Tree cover, flooded, fresh or brackish water;
	Tree cover, flooded, saline water;
	Shrub or herbaceous cover, flooded, fresh/saline/brackish water

3 Methods

I use two complementing approaches to explore the carbon data sets from different angles. In the first part the covariation of carbon and auxiliary variables with burned area is compared on various spatial scales. Firstly, event compositing is used for the analysis on the global scale. Secondly, anomaly time series of carbon data and the auxiliary parameters are compared on the local scale for selected wildfire cases which are scientifically well-documented (see Table 3). Thirdly, the same time series are inspected for four intermediate spatial scales: the Southern Hemisphere, (SH, $0-60^{\circ}$ S,

180° W - 180° E), the larger Australian region including the Southern hemispheric part of Southeast Asia (larger AU region, $0-50°$ S, $98-180°$ E), Australia (AU, $11-48°$ S, $110-160°$ E), and Southeast Australia (SE-AU, $30-40°$ S, $145-154°$ E). In the second part the correlation between carbon and BA data is analysed on these intermediate spatial scales, with the aim to determine the fire signal in different carbon data sets. In analysing the intermediate spatial scales we want to account for the atmospheric transport of the fire signal in the atmospheric observations (CO_2, CO, AOD) which can take place within one month. This loosens the tight spatial coupling of immediate fire site and fire signal. It is the best available strategy that can be implemented without the application of complex trajectory simulations. We focus on Australia for several reasons. The Southeast Australian Bushfires are among the most extreme wildfire events in recent years, and the CO_2 data coverage allows us to study this event. Additionally, CO_2 levels in the Southern Hemisphere have the advantage of being less influenced by anthropogenic point sources and vegetation (Ciais et al. 2019).

3.1 The Behaviour of Carbon and Auxiliary Variables in Relation to Fires

These analyses investigate the relationship between atmospheric carbon and the auxiliary variables during fire events on the global, local, and intermediate scales. We expect to reveal a correlation in time for these parameters. Systematic behaviour could be used to detect enhanced fire carbon emissions and fill gaps in the carbon data sets, which would be particularly convenient for CO_2 data.

3.1.1 Fire Event Composite Anomalies

Event compositing, or superposed epoch analysis, is a tried and tested statistical method to determine the response of one or multiple variables to a particular event (Fischer et al. 2007; Lesk et al. 2016; Nicolai-Shaw et al. 2017; Suji et al. 2018). I apply event compositing to assess global covariation of CO_2, CO, LST, AOD, TWS, NDVI, and L-VOD anomalies during extreme fire events. In the following paragraphs I describe the single steps of computing fire event composite anomalies (FCAs). For a visual abstract of the workflow, see Figure 2.

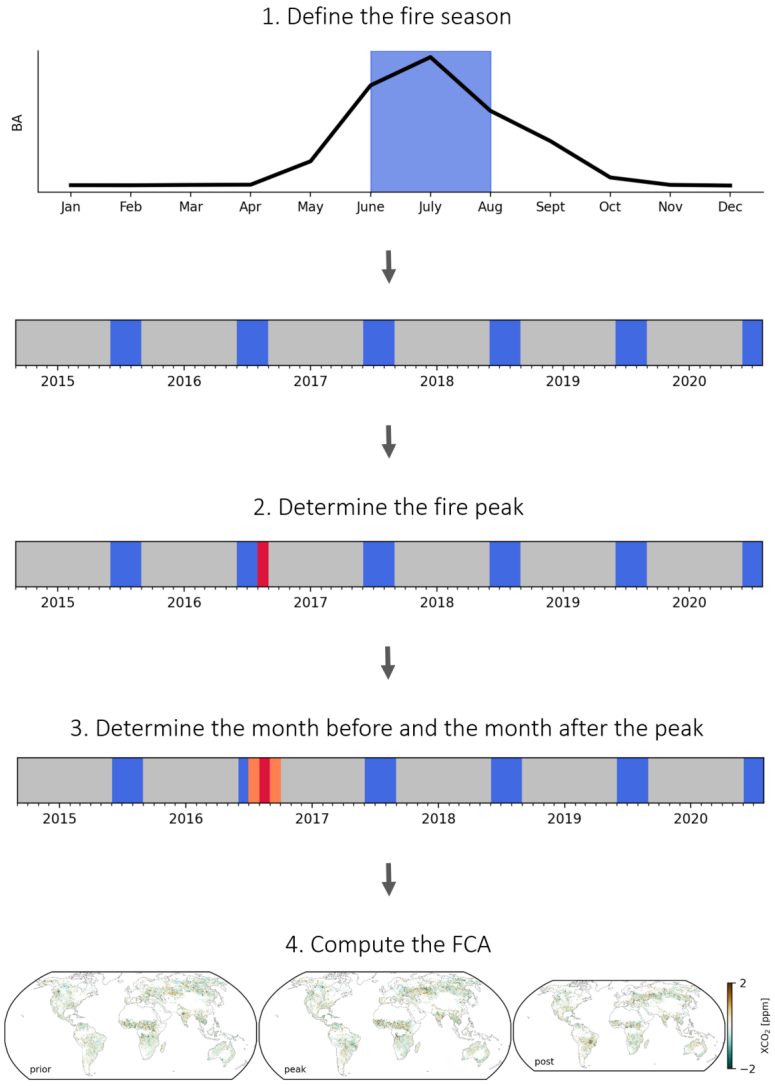

Figure 2: For each grid cell of the BA data set, the mean seasonal cycle is defined and the three months with the highest values defined as fire season (step 1). The most extreme fire month (in terms of BA) over the entire time series is then identified (step 2), as well as the month before and the month after (step 3). Finally, the anomaly at the time of the fire peak is calculated for all auxiliary variables (step 4). Shown here are the CO_2 fire composite anomalies.

1. Define the fire season. In the first step, a fire season mask is created for later anomaly calculations. This is done as it is of interest how extraordinary the parameter values are in respect to the fire season, and not to the entire time series. To this end, I calculate the monthly climatology of original (not deseasonalised) BA data for each grid cell, using the period from September 2014 to July 2020. Subsequently, the climatology values exceeding the 75th percentile threshold are identified, which results in a Boolean mask marking the three months with the highest BA values. This mask is then extended to cover the complete time series.

2. Determine the fire peak. The single most extreme fire event for the entire period is identified according to the maximum value in the original (not deseasonalised) BA

data set. The time of the peak BA value, henceforth called "fire peak", is defined as key time for each grid cell. Then a Boolean mask is created, containing true values when the fire peak occurs, and false values at all other time steps.

3. Determine the month before and the month after the fire peak. In a similar fashion, a pre-fire-peak and a post-fire-peak mask are established, marking the month before and the month after the fire peak occurrence, respectively. With this I intend to characterise the auxiliary parameters' temporal evolution and to examine their role during the build-up and recovery phase of extreme fire events.

4. Compute FCAs. With the help of the mask, FCAs during the extreme fire event are calculated for carbon data and the auxiliary parameters. Since seasonality is removed for all variables as described in section 2.2 *Data Selection and Preprocessing*, FCAs are computed with the anomalies as follows:

$$FCA = X_{fire\,peak} - mean\,X_{fire\,season} \tag{1}$$

where $X_{fire\,peak}$ is the parameter anomaly value at the time of the fire peak and $mean\,X_{fire\,season}$ is the parameter anomaly mean during the fire season. Equivalently, the FCAs one month prior to and one month after the fire peak are computed.

3.1.2 Time Series Analysis

For the local covariability assessment of carbon data and auxiliary parameters I inspect eight regions where exceptional wildfires occurred during the period September 2014 - July 2020. Seven of the eight wildfire incidents are selected based on scientific publications (see Table 3). Additionally, I examine a fire incident in Angola to have a representative case for the African continent. The Angolan wildfire event is, however, not exceptional in terms of frequency, as fires of the same magnitude occur every year in the Angolan savanna. The regions examined differ in their spatial extent. For each region, the time series of carbon data anomalies and auxiliary parameter anomalies are compared. Any repeating patterns in the time series may allow us to distinguish large fires from other sources of carbon variability and could pave the way for an CO_2 gap filling approach.

Table 3: Selection of large wildfire occurrences and estimated carbon emissions. Asterisks link emission estimates and sources where necessary. Emission estimates are in GtC if not indicated otherwise.

Time	Region	Source	Emission Estimate [GtC]	Method
2015	Indonesia	Heymann et al. (2017)	0.204 ± 0.057	obs. (OCO-2)
2015	Siberia	Guo et al. (2019)	$3 * 10 * *$-$8 * 10 * * - 5$	obs. (OCO-2)
2016	Brazilian Amazonia	Withey et al. (2018),	0.008	obs. (bottom-up/top-down)
2017-10	California	Li et al. (2019)*, Garcia et al. (2017)**	max. ΔCO_2: 2 ppm*, 0.003**	obs.s (OCO-2)*, obs. (LiDAR & OLI)**
2017-7/8	British Columbia	Mao et al. (2021)	max. ΔCO_2: 4 ppm	obs. (LiDAR)
2018	California	Rooney et al. (2020)	-	-
2019-11/12	Australia	Byrne et al. (2021)	0.031-0.064	obs. (OCO-2)
2020-1	Australia	Wang et al. (2020)	max. ΔCO_2: 1.5 ppm	obs. (OCO-2)

3.2 Vegetation-dependent Fire Imprint in different Carbon Data

For further insight into the interplay of fires and CO_2 emissions, the correlation of carbon data and BA is examined. This analysis is inspired by Wang et al. (2020), who studied the correlation of wildfire-induced CO_2 enhancements as observed by OCO-2 and modeled wildfire carbon emissions based on the Global Fire Emissions Database, Version 4.1 (GFED4.1) for the Australian mega-bushfires in November and December 2019. Here I inspect the carbon-BA relationship for seven vegetation classes and at the four different intermediate spatial scales mentioned above.

For these areas, the data is processed as follows: I compute the sum of the monthly BA values per vegetation class and monthly means are created for CO_2. With the monthly values for both carbon data sets, spatially weighted area means are calculated and subsequently, the trend is removed. In addition to these two carbon data sets, I introduce a further data set, i.e. corrected CO_2 (CO_2 corr), representing atmospheric carbon. With this data set, we try to enhance the carbon-BA correlation by carving out the fire signal in the CO_2 data. We assume that the most relevant fluctuations in atmospheric CO_2 on a relatively short time scale of months to a few years are caused by the following sources and/or sinks: fires, anthropogenic emissions (from fossil fuel combustion and cement production), land use and land cover change (LULCC), volcanic emissions, and the seasonal cycle of the vegetation. To focus on enhancements caused by fires, all other sources and sinks of atmospheric carbon should be removed from

the CO_2 data. NBP data from the selected DGVMs serve as proxy for the vegetation signal. Spatial sums of the monthly NBP data are calculated and the mean of the seven DGVMs is computed. This multi-model mean of NBP data is then subtracted from the CO_2 data, and the trend is removed from the result. In an attempt to further enhance the fire signal, global anthropogenic emission data (GRACED) is prepared for subtraction. However, the time series of GRACED starts in 2019, leading to an overlap of GRACED and CO_2 data of only 19 months (Jan 2019 - July 2020). Moreover, the years 2019 and 2020 are—due to the COVID-19 pandemic—not representative with regard to anthropogenic emissions, so that any extrapolation could not be considered realistic. For these reasons, we refrain from further pursuing the subtraction of the anthropogenic signal. Yet removing the trend comes close to a correction of the anthropogenic emissions, as they are responsible for the trend to a very large degree. For LULCC and volcanic emissions, data that meet the necessary requirements could not be obtained. However, the LULCC signal is implicitly simulated in NBP data. For a visualisation of the corrected data described in this section, see Figure 3.

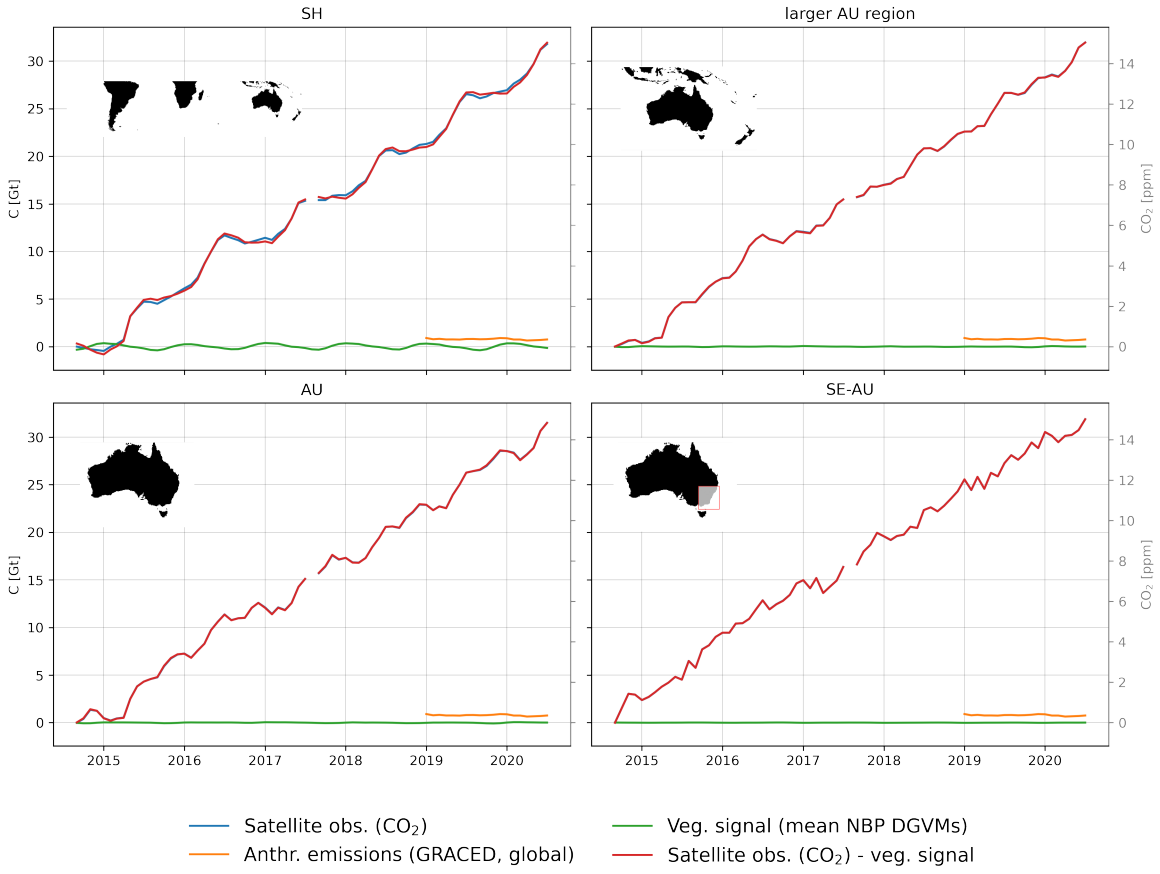

Figure 3: For each spatial scale, the CO_2 data is corrected for the vegetation signal represented by the mean NBP of the seven DGVMs. Anthropogenic emissions are excluded from further analysis due to their short time series. The trend is removed later from the corrected CO_2 data. The CO_2 baseline is removed in this plot and carbon in gigatonnes (left y-axis) is converted to CO_2 in ppm (right y-axis) using a conversion factor of 2.124, following the approach of Ballantyne et al. (2012).

4 Results

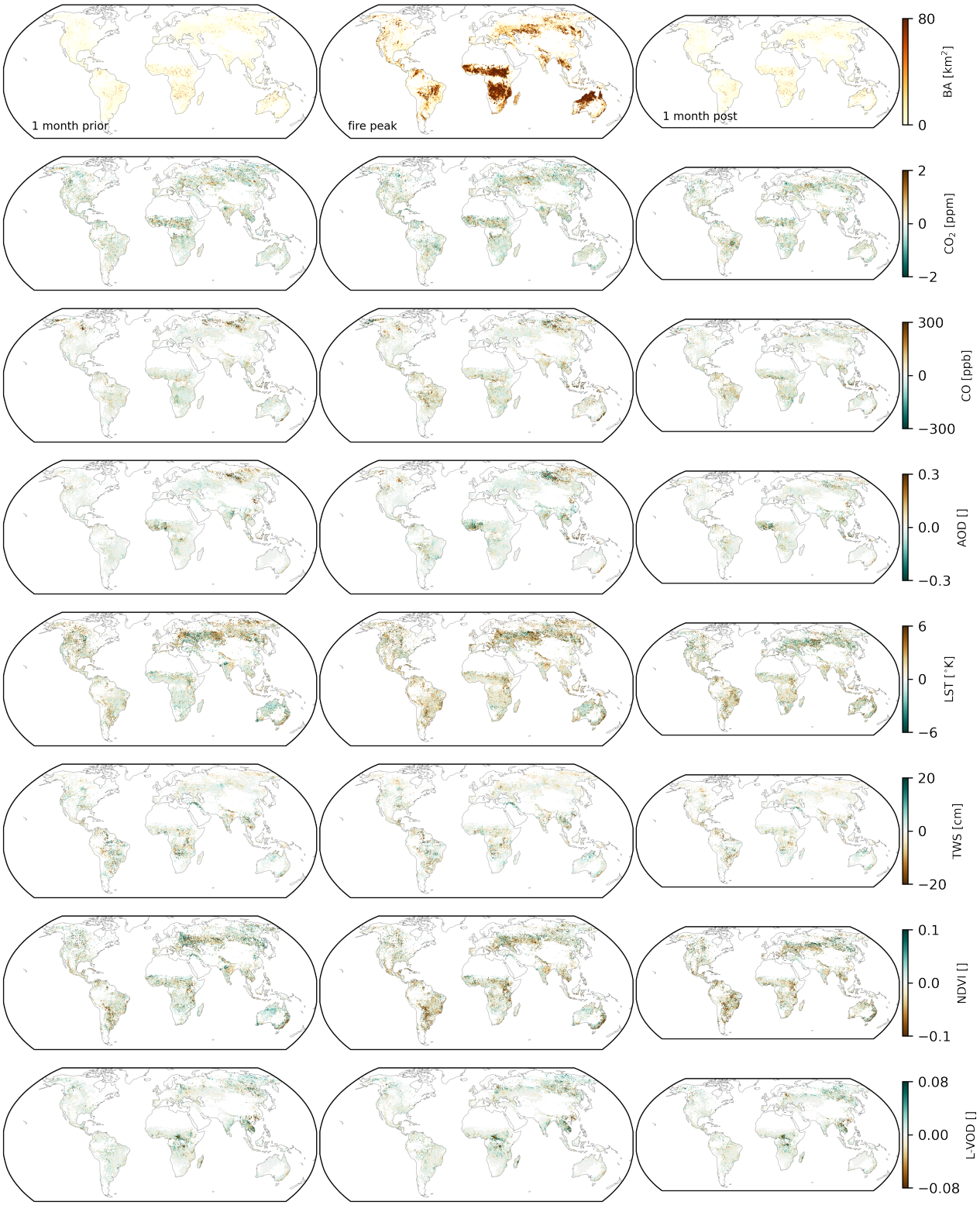

Figure 4: The fire composite anomalies show covariations of BA, carbon, and auxiliary variables in response to an extreme fire event on the 0.25°grid map. Anomalies one month before the fire peak (left column), at the time of the fire peak (central column), and one month after the peak (right column) are depicted. Brown colours indicate anomalies which might be expected in relation to fire, e.g. higher CO_2, or lower NDVI.

Figure 4 demonstrates the global covariation of atmospheric carbon and auxiliary parameters during extreme fire events on the 0.25°grid according to the fire composite analysis. CO_2 does not reveal clear positive anomalies at the maximum fire event. On the global scale, an unambiguous signal cannot be identified. CO_2 anomalies hardly change over the time span depicted, with the exception that CO_2 values are enhanced in South America one month after the fire peak. The pattern of positive CO anomalies correlates rather well with the BA pattern during the fire peak, except that the Western Russian and Central Asian regions do not show any CO increase. Above 60° N, in Alaska, Canada and Northeast Siberia, values are enhanced during the fire peak, but also in the month before. In South America and Southern Africa there is a noticeable increase in CO during and after the fire peak. In Australia, there are more positive CO anomalies during the peak too, but the differences before, during, and after the peak are small. On the African continent, there is no very clear distinction between subtropics and tropics during the peak—as opposed to in BA anomalies—even if there are strong positive CO anomalies, particularly in the Northern subtropics. For AOD, positive anomalies are discernible in the Canadian, South American, Western subsahara African, Indian, Southeast Asian, Northeast Siberian, and Southeast Australian regions. However, most of these patterns can be seen already one month prior to the fire peak. Interestingly, fires in Northern Australia do not seem to enhance AOD noticeably, contrary to fires in Southeast Australia. Among all auxiliary variables, LST show positive anomalies in relation to fire most consistently over the globe, particularly during the fire peak and the month before. An exception to this pattern is Northwestern Australia, where positive anomalies are apparently stronger after the fire peak. The negative TWS anomalies in general agree with the maximum BA during the fire peak. However, Australia again takes on a special role, as there are many positive anomalies there. The NDVI patterns are closely related to those of LST. Negative NDVI anomalies may occur after the maximum fire event, as the example of Australia shows. Yet over all, there is remarkably little temporal evolution in NDVI over the three months. L-VOD anomalies convey no clear pattern and hardly any temporal evolution. The anomalies cannot be related to fire events. In summary, CO and LST exhibit the strongest covariations with fire. There are mixed signals for CO_2 values, which cannot be clearly related to fires. TWS, AOD and the vegetation indices only convey a weak and inconsistent signal in response to fire, particularly L-VOD.

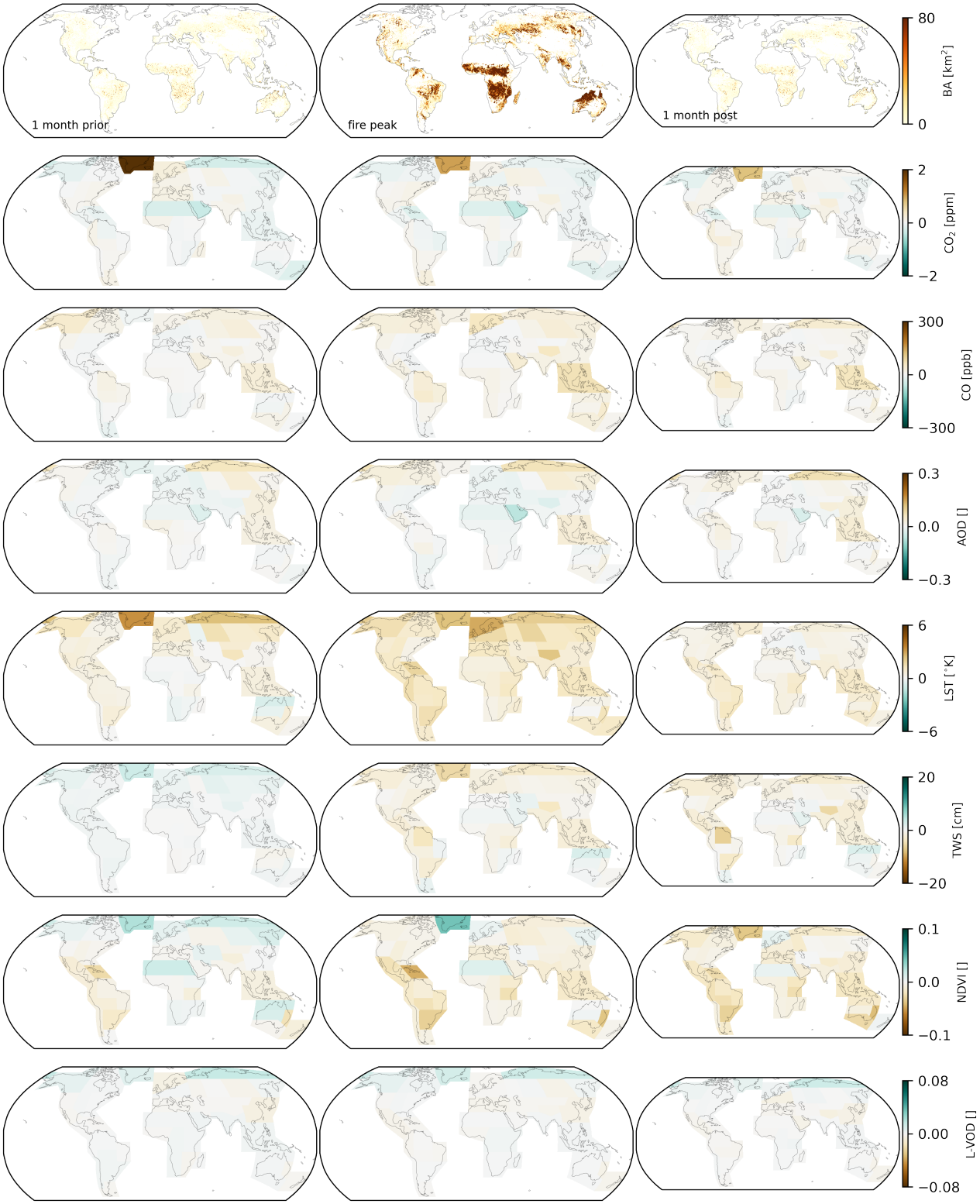

Figure 5: The fire composite anomalies show covariations of BA, carbon, and auxiliary variables in response to an extreme fire event, aggregated across IPCC WGI reference regions. Anomalies one month before the fire peak (left column), at the time of the fire peak (central column), and one month after the peak (right column) are depicted.

In Figure 5, the same data are depicted as in Figure 4, but spatially averaged for IPCC WG1 reference regions, version 4 (Iturbide et al. 2020). These maps help to identify which variables change remarkably over time: LST, the TWS, and the NDVI. On the other hand, CO, AOD, and L-VOD hardly vary over time. Neither does CO_2, with the exception of slightly increased positive anomalies after the fires in South America and the Russian Arctic. Across all variables there are some misleading anomalies, as certain regions (Greenland/Iceland, Northern Europe, Sahara, Arabian Peninsula, West-Central Asia, East-Central Asia, Tibetan Plateau) contain very few data points.

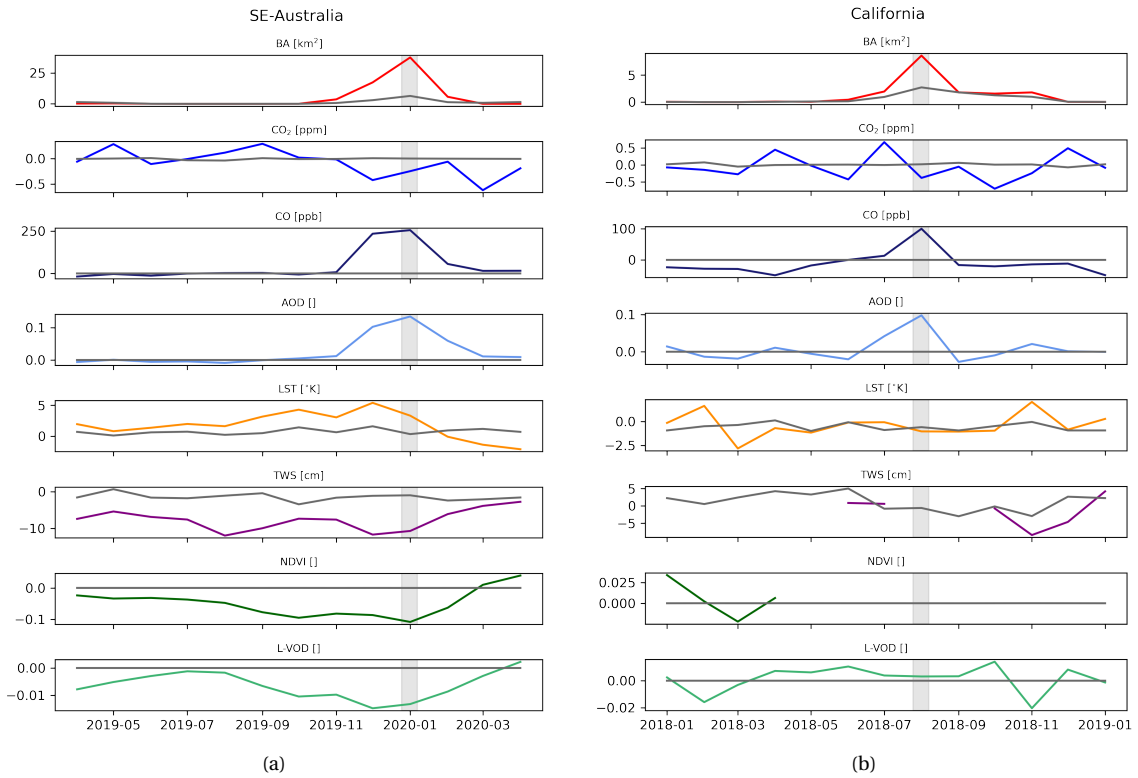

Figure 6: Time series of BA, carbon, and auxiliary parameters' anomalies during an extreme wildfire event in Southeast Australia (6a) and California (6b). Grey lines indicate the parameters' climatology, based on the period from September 2014 to July 2020. The vertical grey bar marks the month of maximum BA, used here as indicator for the fire peak. Note that the y-axes are not of the same scale.

Figure 6 reveals the local behaviour of atmospheric carbon and auxiliary parameters during two selected extreme wildfire events in more detail regarding the temporal evolution. The two cases, illustrating the results of the time series analysis in exemplary fashion, are the 2019-2020 Southeast Australian bushfires (6a) and the 2018 California wildfires (6b). The time series of six more specific events (2015 Indonesia, 2015 Siberia, 2016 Brazilian Amazonia, 2017 California, 2017 British Columbia, 2016 Angola) can be found in the appendix. In the case of the 2019-2020 Southeastern Australian bushfires, a positive or negative peak is visible for nearly every parameter. The exception is CO_2, which does not reveal any particular behaviour upon the wildfire occurrence. CO, by

contrast, exhibits a clear maximum during the fire peak, as does AOD. For LST, the maximum occurs in December 2019, the month before the fire peak, and generally increases since May 2019. TWS is very low during the fire and in the months before, but recovers afterwards. The two vegetation indices convey a very similar pattern: they start to decrease approximately six months prior to the fire event, and reach their low at the fire peak (NDVI) or shortly before (L-VOD). In the case of the 2018 California wildfires, the parameters' covariation is more ambiguous. Only CO and AOD demonstrate a clear peak at the fire maximum. For CO_2, no particular reaction to the wildfire is visible. There is a positive CO_2 anomaly in the month before the fire maximum, yet it is not much more pronounced than the other positive anomalies in 2018. The remaining parameters do not show any specific behaviour related to fire. Unfortunately, there are considerable gaps in the data of 2018 in California for NDVI and TWS. The other six cases examined reveal mixed results. CO_2 does not show extraordinarily high levels upon the fire in any of the cases. CO and AOD demonstrate a clear reaction in four out of the six cases, it might occur one month before, one month after, or during the fire peak. Also in four cases, LST is enhanced during the fire peak. For all cases TWS data does not cover the entire year, so that it is difficult to make a statement about covariability. NDVI decreases during the fire peak or one month later in three out of the six events. L-VOD does not exhibit any systematic fire response. For the eight inspected cases, CO_2 does not demonstrate consistent covariability with the fire event, CO and AOD generally peak around the fire maximum, LST are enhanced during and before the fire in five out of eight cases, TWS data do not allow any conclusion, and the vegetation indices drop in some cases, but not consistently.

Time series of BA, carbon, and the auxiliary parameters on the intermediate spatial scales are depicted in Figure 7. It is difficult to identify interlinked behavioural patterns in the Southern Hemisphere (7a). For the larger Australian region (7b), such faint interconnections become apparent. At the end of 2019—i.e. at the time of the extreme Southeast Australian bushfires—positive CO, AOD, and LST anomalies occur, while TWS, NDVI, and L-VOD exhibit negative anomalies. CO_2 anomalies are weakly positive, but lie just on the threshold of one standard deviation. The same pattern emerges more clearly when the spatial extent is decreased to Australia (7c), with CO_2 anomalies just above the one standard deviation threshold. For the still smaller spatial excerpt of Southeast Australia (7c), there is a strong fire signal in all variables but CO_2.

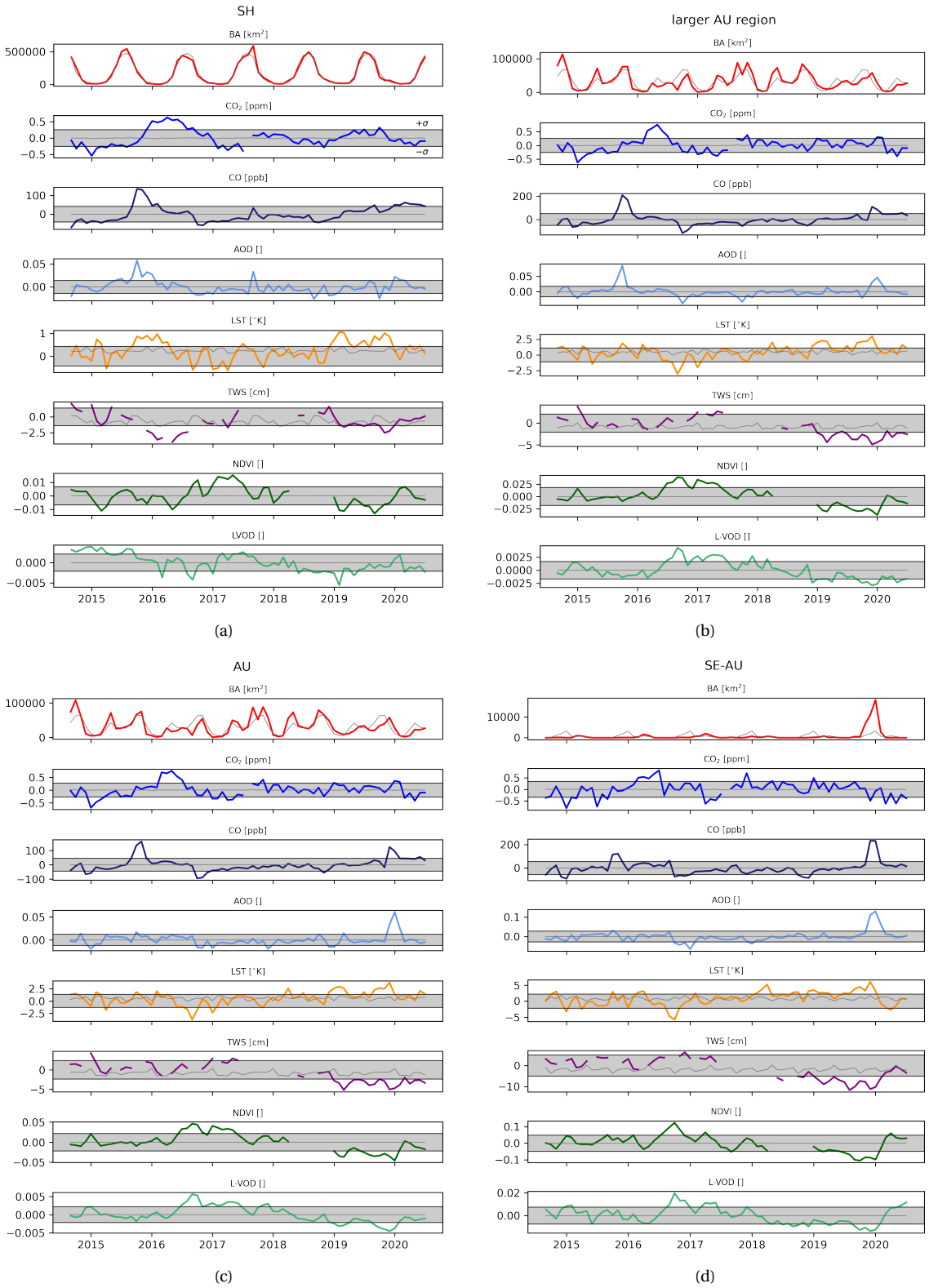

Figure 7: Time series of BA, carbon, and auxiliary parameters' anomalies from September 2014 to July 2020 on the Southern Hemisphere (7a), in the larger Australian region (7b), Australia (7c), and Southeast Australia (7d). Grey lines indicate the parameters' climatology based on the depicted period. The horizontal grey band represents the range from minus to plus one standard deviation. Note that the y-axes are not of the same scale.

Figure 8 shows the statistical distribution of significant correlation values of carbon and BA per vegetation class. Significance implies a p-value lower than 0.05 throughout the thesis whenever significance is mentioned. In this overview, it is apparent that the correlations are highest for the largest spatial scale and become weaker with decreasing spatial scale. For the Southern Hemisphere, the median values are high (CO_2: 0.683, CO_2 corr: 0.758, CO: 0.461), as are the number of significant correlations (CO_2: 6, CO_2 corr: 6, CO: 7 out of 7). For the larger Australian region there are only two significant values for each CO_2 and CO_2 corrected, while all seven correlation values are significant for CO. Concerning CO, there is no change in significant values between the larger Australian region and Australia, where also all correlation values are significant. The significant correlation values for CO_2 and CO_2 corrected, however, increase from two to six at this decrease in spatial scale. The median values per carbon class are in a very similar range for both regions (CO_2: 0.288, CO_2 corr: 0.311, CO: 0.472 for the larger Australian region, CO_2: 0.310, CO_2 corr: 0.322, CO: 0.460 for Australia). For Australia, the spread in Pearson r values is large for all carbon species, as indicated by the outliers. For the smallest region, Southeast Australia, there again is a drop in significant values for all carbon classes to only one value for both CO_2 and CO_2 corrected, and three for CO. The Pearson r value for CO_2 and CO_2 corrected are 0.259 and 0.261, respectively, and with a value of -0.246, the median for CO is negative. In general, median correlation values are high for the Southern Hemisphere and decay with decreasing spatial scales. Median correlation values are higher with CO_2 and CO_2 corrected than with CO for the Southern Hemisphere and Southeast Australia, but lower for the two medium spatial scales. Correlations with CO_2 corrected are slightly higher than with CO_2 throughout all spatial scales.

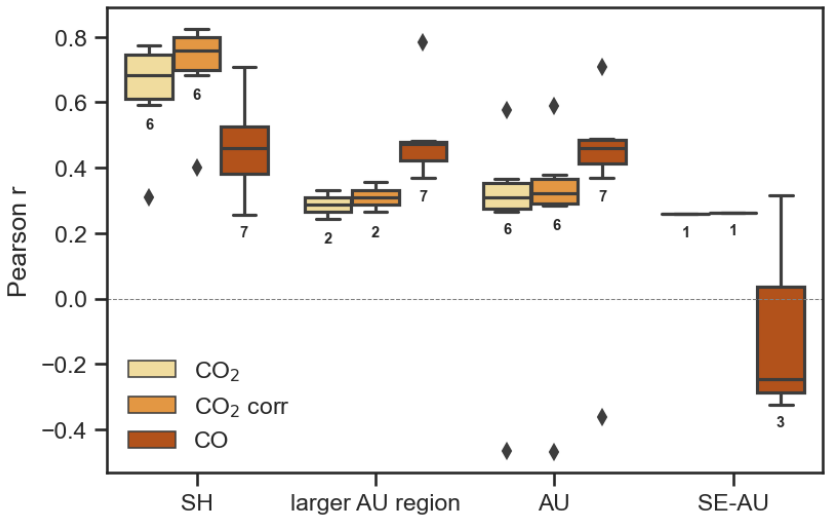

Figure 8: Statistical distribution of significant ($p < 0.05$) Pearson r values for the correlation carbon-BA per vegetation class. The numbers beneath the boxes indicate the number of significant correlations.

A more detailed view of all correlation values per vegetation class is presented in Figure 9. We can infer from this figure which vegetation classes provide high, and which provide low or insignificant correlations. For the Southern Hemisphere, CO_2 and corrected CO_2 data demonstrate higher correlations for most vegetation classes but one ("tree evergreen"), whereas for the larger Australian and the Australian region, the correlations with CO are higher. There are too few significant values for Southeast Australia to draw a clear picture. Vegetation classes that systematically show higher correlation values across all spatial scales and carbon classes do not exist. However, it can be noted that "vegetation flooded" yields the most significant correlation values (in terms of numbers) and they are generally comparatively high, with the exception of CO in the Southern Hemisphere. "Sparse vegetation" is the class with the least significant values, as there are no significant values for CO_2 and corrected CO_2 on any spatial scale. All carbon classes correlate negatively with BA in the vegetation class "crop" for Australia. "Tree deciduous" and "tree evergreen" display comparatively high correlation values for CO in the Southern Hemisphere and Southeast Australia, but in no other case. In summary, this figure shows that the correlation of atmospheric carbon and BA is a function of the spatial scale as well as the vegetation class.

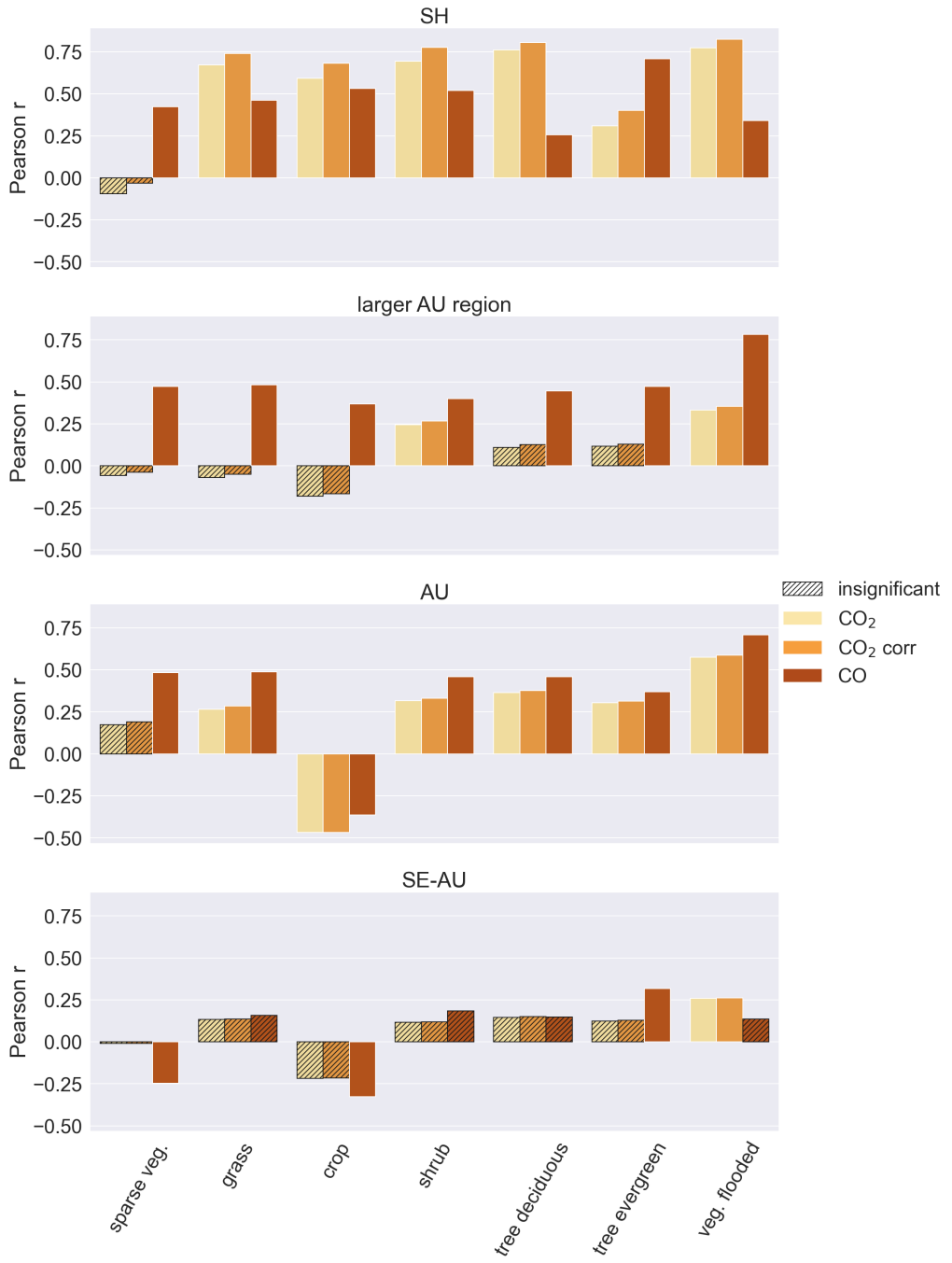

(a)

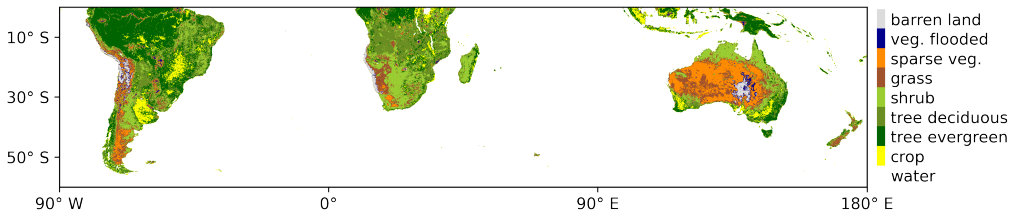

(b)

Figure 9: Pearson r values for the correlation carbon and BA in vegetation class (Figure 9a). Hatched bars indicate insignificant ($p \geq 0.05$) values. Below (Figure 9b) is the distribution of vegetation classes on the Southern Hemisphere.

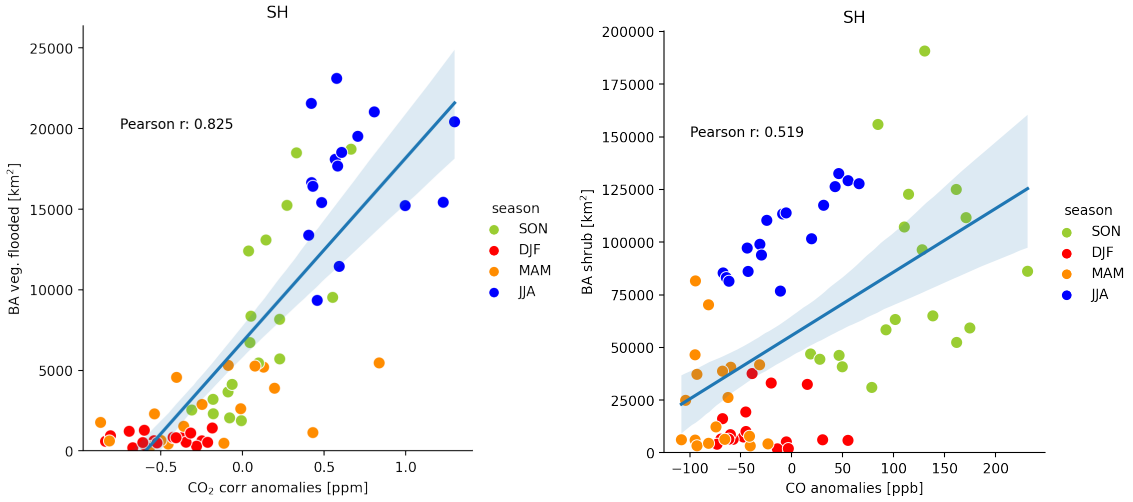

Figure 10: Correlation and linear regression model fit of BA per vegetation class and atmospheric carbon anomalies exemplified by two specific cases for the Southern Hemisphere. The seasonal distribution is mapped: green for austral spring (Sept, Oct, Nov), red for summer (Dec, Jan, Feb), orange for autumn (Mar, Apr, May), and blue for winter (June, July, Aug).

Figure 10 illustrates what some of the better correlations of BA in vegetation class and carbon would look like for the Southern Hemisphere. Figure 10a is the prime example of a good linear correlation in this setting. It shows the correlation of BA in "vegetation flooded" and corrected CO_2. Figure 10b displays the correlation of BA in "shrub" and CO, where the Pearson r value is lower and the linear component is less pronounced. Instead, a cyclic component related to the seasons is apparent, with generally low BA and CO values in summer and autumn, increasing BA and CO values in winter, and a peak and subsequent decrease in BA and CO values in spring. This pattern is common among correlations with CO in the Southern Hemisphere.

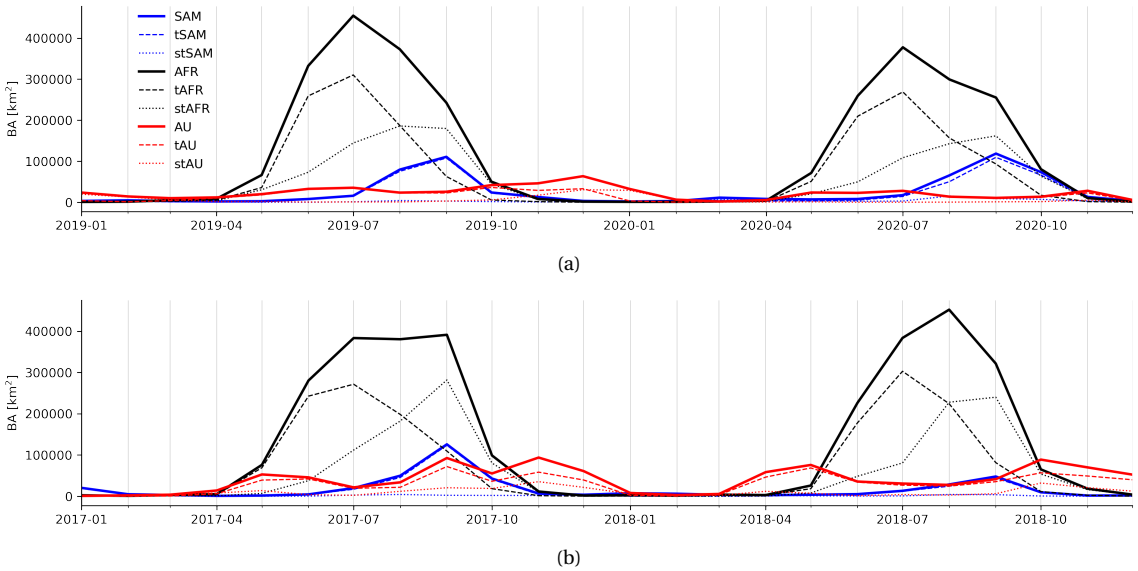

Figure 11: Fire seasons on the Southern Hemisphere according to monthly sums of BA for the years 2019 and 2020 (Figure 11a) as well as 2017 and 2018 (Figure 11b). Depicted are fire seasons for tropical, subtropical, and entire South America (tSAM, stSAM, SAM), tropical, subtropical, and entire Africa (tAFR, stAFR, AFR), and tropical, subtropical, and entire Australia including the maritime continent (tAU, stAU, AU).

The fire seasons as indicated by BA are presented in Figure 11 for the individual Southern hemispheric continental regions. Africa is the largest contributor to total BA on the Southern Hemisphere, where BA peaks around 400'000 km^2, while peaks of BA in South America and Australia are of smaller magnitude of approximately 100'000 km^2 each. The BA peak in tropical Africa in July is usually larger than the BA peak in subtropical Africa, which occurs around September. The peak of the African fire season clearly lies in the austral winter months. There is barely any BA in subtropical South America, so that the peak in total South American BA in spring (Sept) is largely determined by the tropical BA. For the four years inspected, there is no single annual peak in BA for the Australian and South Asian region. Maximum BA values are reached in late spring or summer months (Oct/Nov/Dec), although values in late autumn (May/June) may rise almost as high.

5 Discussion

5.1 The Behaviour of Carbon and Auxiliary Variables in Relation to Fires

5.1.1 The Global Scale

The fire composite analysis yields mixed results concerning systematic changes in behaviour of carbon and auxiliary parameters in connection to extreme fire events on the global scale. Particularly, CO_2 anomalies on the $0.25^\circ \times 0.25.^\circ$ grid maps do not convey a spatial pattern related to BA. The fact that they hardly change over the three months depicted makes it seem as if CO_2 observations were generally fire-independent. Although the regional anomaly aggregation grants some latitude as to the spatial distribution of the fire signal in the CO_2 data, the respective maps do not show clear patterns corresponding or slightly shifted to BA patterns, which could have been explained by transport via the general atmospheric circulation. CO and AOD data do not show a pronounced fire signal either. LST demonstrates good accordance with BA patterns on the high-resolution map during and prior to the fire peak, especially in the Eastern European, Siberian, and Russian-Far-East regions. In addition, the region maps indicate a fire-related temporal evolution, with most pronounced positive anomalies during the fire month in all regions. This is not surprising, as this climatic variable plays an important role in the fire build-up phase, which is often related to heat and drought conditions (e.g. Brando et al. 2019; Jolly et al. 2015). Such co-occurring climate drivers and/or hazards are also described as "compound events" (Zscheischler et al. 2018). TWS seems to be a little less involved in the build-up, and yet obviously related to fires, since negative anomalies in the aggregated maps are increased during and after the fire peak moth. Similarly, NDVI shows increased negative anomalies during and after the fire peak. In L-VOD data a fire response is not discernible.

These results raise the question of what role the temporal evolution plays and what can be concluded from it. Several parameters (CO_2, CO, AOD, L-VOD) do not display a distinct change over time. The fundamental idea of the composite analysis is to identify covariation based on spatial anomaly patterns which resemble the BA distribution during the fire peak, and which strikingly differ from the anomaly patterns before and after the peak. However, defining the fire peak at maximum BA does not imply that there are no fires before and/or after the peak. For regions with long fire seasons, or in the case of extraordinarily long-lasting fires, it cannot be inferred that constant patterns indicate

fire-independence. Furthermore, there may be reasons why the anomaly peak occurs in the month after or in the month before the fire peak, e.g. in the case of LST, as discussed in the previous paragraph. Therefore, covariation cannot be excluded based on the temporal evolution of fire composite anomalies. Aggregating across IPCC WG1 v4 reference regions does not make fire signals in the atmospheric data more explicit, but instead reveals clearer differences in the temporal evolution for LST, TWS, and NDVI, which were difficult to discern in the 0.25°grid maps. In summary, a systematic behaviour of carbon and auxiliary variables in respect to fires is not evident from the grid maps, while the region maps indicates a likely fire-dependent development over time for LST, TWS, and NDVI.

5.1.2 The Local Scale

The analysis of the parameters' temporal evolution for specific wildfire events reveals that, on the local scale, more auxiliary parameters may covary with the fire indicator BA. This applies perfectly to the case of the Southeastern Australian bushfires in 2019/2020. The unambiguous fire signal in all but the CO_2 variable suggests that signals might be highly site-specific. The parameters can be distributed into two groups: TWS and the vegetation indices show anomalously low values for several months prior to and during the fire, and recover afterwards. Similarly, LST exhibits a gradual increase and peaks one month before the fire maximum. This first group of parameters is apparently involved in the initiation phase of fires. By contrast, AOD and CO reveal clear positive anomalies during the fire peak month, which can be interpreted as instantaneous reactions to the fire. The site-specific character of fire-related behaviour in the auxiliary parameters is further underlined by the case of the 2018 Californian fires, where CO and AOD are the only parameters with an apparent fire response. These two parameters also show peaks for most of the other examined cases, though not necessarily simultaneously with BA, but possibly one month before or one month later. Similarly, LST is enhanced before and during the fire peak in most cases. The other parameters do not exhibit a consistent fire response. According to the local time series analysis CO, AOD, and LST are the variables that covary relatively reliably with fire on the local scale.

5.1.3 The Intermediate Scales

Striking differences emerge from the comparison of the parameters' time series for the intermediate spatial scales. While the variables' behaviour cannot be associated with fire events on the Southern hemispherical scale, this attribution is possible for the smaller spatial scales. CO_2 stands out in its behaviour from the other variables. Most of them demonstrate an increasing fire response with decreasing spatial scale, whereas the CO_2 fire signal peaks for the Australian spatial excerpt and is not visible at all for the smallest spatial section, Southeast Australia. Also, for CO_2 the fire signal is generally weaker than for the other variables, for which anomalies lie clearly outside the ± 1 standard deviation range. CO_2 differs from CO and AOD, the two other atmospheric parameters, in the same ways. Their larger relative departure from background levels is likely responsible for this phenomenon. Overall, the spatial extent of the area inspected plays a major role for the behaviour analysis of carbon and auxiliary variables in relation to fires, particularly regarding CO_2. It would be interesting to find out if there is a generally applicable optimal scale for fire signal detection in CO_2 data. Our analyses suggest this might be the subcontinental scale, spanning a few thousand kilometres in latitude and longitude.

Horizontal transport in the atmosphere is probably the primary cause for this dependence on the spatial scale. Mesoscale atmospheric mixing typically occurs in spatial scales of ten to a few hundred kilometres and within a few hours to a few days (Lin 2007). The synoptic scale includes mixing processes such as tropical and mid-latitude cyclone systems that usually have an extent of a few thousand kilometres and a lifetime of days to weeks (Rohli et al. 2015). Given that on these spatial scales horizontal atmospheric transport takes place within a short time span, it does not come as a surprise that fire signals in monthly resolved and regionally averaged CO_2 data are difficult to detect. In the case of the FCA analysis as well as the local time series and the time series averaged across Southeast Australia, the signal may be transported away from the immediate location of the fire. For larger areas it is more likely that the signal stays within the prescribed borders, as planetary scale atmospheric mixing processes operate over weeks to months (Rohli et al. 2015). Intra-hemispheric mixing may occur within a few months (Seinfeld et al. 2016) and inter-hemispheric mixing within a bit more than a year (Seinfeld et al. 2016; Patra et al. 2009). According to this hypothesis, fire signals should increase for larger spatial scales. This is confirmed by the correlation analyses, as discussed in section 5.2.1.

5.1.4 Previous Work

There is a body of work investigating the relationship of climate anomalies and fires using composite analysis on regional scales. However, these analyses focus on fire-conducive conditions related to droughts (O'Donnell et al. 2011; Rao et al. 2019), and to climatic teleconnections (Hessl et al. 2004; Skinner et al. 2008; Cardil et al. 2021). Except for the computation of climatic teleconnections indices, none of the data sets in these studies come from remote sensing. Rao et al. (2019) and O'Donnell et al. (2011) find a link of fire occurrences to anomalously dry (and hot) conditions. Unfortunately, this is not evident in the selected local time series of TWS data, as there are many gaps in this data set. However, for five out of the eight cases inspected, the LST time series support these findings. It is more challenging to establish this link between fires and TWS/LST on the global scale by means of FCAs. For TWS, again, the gaps in the data set obstruct a clear signal extraction. In the LST time series it is visible that often higher than normal values extend to the months before and after the fire peak, which is also mirrored in the FCA analysis, where the differences in anomalies before, during, and after the peak are rather subtle. To the best of my knowledge, a fire composite study including atmospheric CO_2, CO, or aerosol observations, or vegetation indices does not exist. Therefore, there is no reference point whether the FCAs are in a common range, or whether the data could be refined with more elaborate methods to identify covariations of these parameters with fires. Of the FCAs studied, CO is the most likely to covary with BA on the global scale. Scientific literature suggests that TWS and LST data also covary with BA, however, further data processing steps might be necessary to confirm this for the small scale and establish it for the large scale using my methods. For the other parameters, the FCAs indicate weak or no fire-related behaviour. In particular, the absence of a fire signal in the CO_2 data not only in the FCAs, but also in the local time series is remarkable. This complete absence on the large and small scale makes it impossible to distinguish fire emissions from other sources of CO_2 within the data set. Moreover, CO_2 data density must be sufficiently high and the covariance with other parameters must be pronounced in order to successfully train a gap-filling algorithm. Since both conditions are not fulfilled, developing a multivariate gap-filling approach based on this work is not possible.

5.1.5 Limitations

A few limitations apply to these approaches which render the co-dependent behaviour analysis difficult. A major hindrance affecting most data sets is the lack of data due to

diverse restrictions, e.g. the sparse sampling density in time, cloud interference, instrument failure, or a gap between original and follow-on missions. Data quality of any satellite observation is subject to sensor ageing and the skill of retrieval algorithms. Moreover, the data sets differ in their spatial and temporal aggregation methods. A meaningful comparison of eight variables, each with its own sources of uncertainty, is thus not straightforward. As mentioned above, rapid atmospheric transport is very likely a further factor hampering this type of analysis with regard to the atmospheric variables. The carbon and AOD signals might be diluted rather quickly, depending on the spatial scale inspected. Moreover, there are some limitations specific to the satellite observations of CO_2. Smoke plumes often obscure the measurements at wildfire locations, leading to a lack of data where atmospheric carbon enhancements are expected to be highest (Wang et al. 2020; Mao et al. 2021). For OCO-2 CO_2 observations, Connor et al. (2016) report net variable errors usually < 1 ppm over the oceans and ranging between 0.5 - 2.0 ppm over the land. Considering that enhancements expected from large wildfires range between 1.3-2.0 ppm (Li et al. 2019; Wang et al. 2020), this error is large and may additionally prevent reliable wildfire signal detection. Furthermore, it is debatable whether the atmospheric column-average of CO_2 values is an appropriate variable for fire signal detection. It is possible that elevated values near the Earth's surface due to fires are masked in this way. Another source of uncertainty is rooted in the spatial interpolation method applied to generate the multi-instrument CO_2 product used in this thesis.

5.2 Vegetation-dependent Fire Imprint in different Carbon Data

The characteristics of satellite carbon observations related to fires can be elaborated using the box plot and the bar plot, which together present a summary of the BA-carbon correlations. In general, the range of correlation values is large. Evidently, in some cases the correlations reach very high values. However, if the spatial scale is too small (with a longitudinal and latitudinal extent of a few hundred kilometres as in the case of Southeast Australia), neither CO_2 nor CO correlate well with BA. Another distinct feature emerges from the plots: corrected CO_2 data produce higher correlation values than original CO_2 data. In the following paragraphs, the differences in the three carbon data types are discussed in more detail.

5.2.1 Characteristics of CO_2 and corrected CO_2

Correcting CO_2 values for the vegetation signal is successful, as it enhances the BA-CO_2 correlation on every spatial scale and for all vegetation classes, with only one exception ("crop", AU). The greatest improvements are achieved for the Southern Hemisphere. From the large to the smaller spatial scales the differences between CO_2 and corrected CO_2 decrease. The spatial scale is generally more relevant than vegetation classes regarding the quality of the BA-CO_2 correlations, both for the original and the corrected data. Correlation values are good for the Southern Hemisphere—noticeably better than correlations with CO—, but disintegrate quickly towards the smaller spatial scales. Atmospheric transport most likely plays a decisive role in this situation, too, and is responsible for the fact that the location of monthly trace gas observation and the location of trace gas origin are not necessarily the same. In the case of the Amazonian region, for example, long-range transport, convergence into the Central Basin, and the location of the ITCZ decisively shape the composition of the atmosphere and consequently the biosphere-atmosphere interactions in this region (Andreae et al. 2012). Similar general and locally specific processes may influence the atmosphere above Australia. Yet atmospheric transport alone cannot fully account for the difference in significant values between the larger Australian region including Southeast Asia, and the smaller region of Australia only. Possibly, the special role of Southeast Asia in the climate system is partly responsible for this discrepancy, e.g. its high sensitivity to changes in the El Niño Southern Oscillation. Fuller et al. (2006) published strong correlations of fires in forested insular Southeast Asia with the Southern Oscillation Index and the Niño 3.4 index. Similarly, Wooster et al. (2012) report strong positive statistical associations between the cumulative NINO3 anomaly and active fire counts on Borneo, taking into consideration fire subseasons separated by monsoons. These highly specific climatic processes in Southeast Asia differ from those in Australia, which might cause conflicting correlation signals if the two regions are inspected as one unit.

5.2.2 Characteristics of CO

The plots underline that the strength of the correlation depends heavily on the vegetation class for CO in the Southern Hemisphere, as can be interpreted from the large spread. The median values for correlations with CO are of similar magnitude in all spatial scales, except Southeast Australia. This indicates that the vegetation class controls correlation scores for CO rather than the spatial scale. It suggests that fires in spe-

cific vegetation classes—and ergo in specific regions in the Southern Hemisphere—enhance CO values more than fires in other classes. BA in the vegetation class "tree evergreen" has the highest correlation with CO in the Southern Hemisphere.

5.2.3 The Influence of Vegetation Classes on Carbon Observations

The vegetation classes seem to affect the carbon observations differently. In contrast to the Southern Hemisphere maximum correlation CO-BA in "tree evergreen", the same correlation ranges among the lowest on the two middle spatial scales. It is surpassed by correlations with BA in "vegetation flooded", which also yields highest correlations with CO_2 and corrected CO_2 throughout all spatial scales. This is interesting, as there are no major areas of "vegetation flooded" in the Southern Hemisphere. There are no noteworthy occurrences of "vegetation flooded" in Africa, which is a common feature of both vegetation classes with the highest correlations ("tree evergreen" and "veg. flooded"). It suggests that biomass burning in Africa has a subordinate influence on atmospheric carbon monoxide levels. This might be linked to Edwards et al. (2006)['s] findings, who analysed the interannual variability of CO on the Southern Hemisphere using satellite observations. They demonstrate that southern Africa and South America usually produce the largest share of CO, yet the most significant interannual variability is caused by varying fire activity from the maritime continent and northern Australia. The low Pearson r values of the vegetation classes "crop" and "shrub" might be explained by the little biomass contained in these classes. In the case of crop, it can furthermore be assumed that extended fire management measures are taken to avoid large fires. However, low correlations for the tree vegetation classes on the largest spatial scale do not support the hypothesis that low fuel vegetation classes generate low, and fuel-rich vegetation classes generate high correlations. For the Southern Hemisphere it becomes clear again that different vegetation classes achieve a very different effect on correlations of BA with CO and on correlations with CO_2, as BA in "tree deciduous" reveal a strong correlation with CO_2 and corrected CO_2, while it represents the minimal correlation with CO. On the other hand, BA in "tree evergreen" has minimal correlation with CO_2 and corrected CO_2, and maximal correlations with CO.

5.2.4 Seasonal Fluctuations in CO_2 Levels

To understand the seasonality in the bivariate distribution of BA and carbon it is necessary to make a brief digression into the seasonal distribution of atmospheric CO_2

and CO. The main driver of seasonality in CO_2 on the large scale is the net ecosystem production (e.g. Pearman et al. 1980; Bacastow et al. 1985), which largely depends on terrestrial vegetation. Accordingly, atmospheric CO_2 values are high in winter, when the vegetation uptake is at its minimum, and in summer they are low. The Southern hemispheric fire season augments this signal, as the maximum BA is reached in winter. The reason why we have decided not to remove the seasonal signal from the carbon data is that fires also have a seasonality, and thus contribute to this signal. For the correlations with original CO_2 data, it therefore remains unclear to what degree the correlation is due to fires, and to what degree it is due to the seasonal vegetation signal. This circumstance is taken into account with the correction of the CO_2 values for the vegetation signal. Expected and presented results for the seasonal CO_2 distributions in relation to seasonal BA distributions correspond well.

5.2.5 Seasonal Fluctuations in CO Levels

Like CO_2 concentrations, CO concentrations are generally high in winter and lowest in late summer (Khalil et al. 1990). This seasonal distribution is the result of the interplay between CO production, transport, and removal. Anthropogenic CO sources are fossil fuel and biomass combustion, waste incineration, and industrial processes; natural CO sources are oceans, soils, plants, and forest fires. In addition, the oxidation of CH_4 and other hydrocarbons contributes a major part to atmospheric CO levels. CO is mainly removed from the troposphere by reaction with the OH hydroxyl radical, a part is transported and oxidised in the stratosphere, and a still smaller portion is taken up by soils and oceans (Badr et al. 1995). The CO seasonal distribution is thus coupled to the seasonality of OH. Reduced solar radiation, water vapour, and ozone during winter cause OH levels to drop (Khalil et al. 1990), and subsequently, the utilisation of CO by reaction with OH is lower, leading to the enhanced winter CO concentrations. Additionally, more stable atmospheric conditions in winter cause reduced transport to the stratosphere through convective and turbulent processes (Seiler 1974). The seasonal cycle of CO is also affected by the seasonality of sources (Khalil et al. 1990). This theoretical CO seasonal cycle is merely partly confirmed in the exemplary correlation plot. Very low CO values indeed occur in summer and autumn, but they reach their maximum in spring, not in winter. This result agrees with the findings of Andreae et al. (2012), who document strong influence of biomass burning emissions on atmospheric CO levels over the Amazon Basin during the late dry season in austral spring, while they report only low enhancements of CO mixing ratios during the late wet season in austral autumn. This is in accordance with the fire season in spring for tropical South

America. However, if biomass burning is the dominant driver of CO variability in the Southern Hemisphere, how is it possible that maximum CO values do not occur simultaneously with maximum BA values in winter? Again, I hypothesize that fires in certain regions (and vegetation classes) on the Southern Hemisphere may affect CO concentrations more strongly than fires in other regions (and vegetation classes). In the case of the correlation in Figure 10b, this could mean that BA in vegetation class "shrub" peaks in winter largely due to high values on the African continent, while "shrub" fires do not release major amounts of CO into the atmosphere. Rather, CO values rise in spring, when certain vegetation classes, e.g. "tree evergreen", burn in South America, Southeast Asia, and Australia.

5.2.6 Limitations

Limited data availability confines the informative value of these analyses in general. More specifically, the correction of CO_2 data is restricted to the vegetation signal, since suitable data records for anthropogenic, subaerial volcanic, and LULCC emissions are not available. Nevertheless, the results demonstrate that it is worthwhile to undertake the correction of the CO_2 data in order to enhance the fire signal. While this curtailed approach yields good results for the Southern Hemisphere, the noise in the BA-CO_2 correlations on the smaller spatial scales must be further reduced by correcting for other influences. Potentially, correlations with in this way corrected CO_2 data could equal or even exceed CO correlations. Anthropogenic point sources certainly skew the correlations on the regional scale, as do volcanic emissions. (Schwandner et al. 2017), who investigated local CO_2 sources with satellite data from OCO-2, find persistent anthropogenic CO_2 enhancements over the city of Los Angeles of 4 - 6 ppm, and enhancements from the Yasur volcano (Vanuatu) eruption of 3.4 ppm. Both these signals are large compared to the maximum enhancements caused by wildfires (1.3-4.0 ppm) as reported by Li et al. (2019) and Mao et al. (2021). On the global scale, the CO_2 flux from active crater fumaroles and plumes is estimated to be approximately 0.014 - 0.024 Gt carbon per year (53 - 88 Tg CO_2 per year) as reported by Fischer et al. (2020), yet the authors also point out that the less well described diffuse degassing via soils, volcanic lakes and volcanic aquifers could mount to the same annual emissions. Still, these emissions are rather low relative to recent global fire emission estimates of about 2 Gt carbon per year (Zheng et al. 2021; Wees et al. 2022). On the other hand, annual anthropogenic emissions, including land use changes, currently exceed 10 Gt carbon (Friedlingstein et al. 2020). Separating anthropogenic and natural land use change emissions, as well as fire and land use change emissions is extremely difficult. Large

uncertainties are related to CO_2 flux estimates from LULCC, originating from uncertainties in underlying LULCC maps, different complexity, assumptions, and set ups of models, lack of observational constraints, and inconsistencies in common terminology (Pongratz et al. 2021). Other data are also subject to great uncertainty, such as the NBP estimates from the DGVMs, which may strongly differ from one another. A further important constraint is that the BA-carbon correlation is a crudely simplified measure for a highly complex interrelation. Various factors not considered in this thesis may influence the correlation, which underlines the well-known fact that correlation does not equal causality.

5.3 Synthesis

In combination, these results have a few implications for the estimation of fire CO_2 emissions based on satellite observations. The correlation analysis underlines that the vegetation classes play a crucial role in the determination of fire CO_2 emissions. The FCA analysis indicates that neither CO_2 data nor CO data reveal a fire signal on the global scale. According to time series and correlations, the fire response is more pronounced in CO than in CO_2 data on intermediate spatial scales. Focusing on CO measurements can thus be an interesting alternative to estimate global annual CO_2 emissions. van der Velde et al. (2021) demonstrated that CO data can be used to infer CO_2 emissions with the help of empirically derived vegetation-dependent CO_2 and CO fire emission factors and their ratios for the regional scale, and Zheng et al. (2021) conducted a similar study for the global scale. However, emission factors may differ considerably even within the same vegetation class (Wiggins et al. 2021). Furthermore, CO to CO_2 emission ratios cannot be readily extrapolated from small to large scales, as our analyses suggest CO observations correlate better with BA on the medium scales, yet on the large scale CO_2-BA correlations perform much better. For these reasons I would take the results of the studies mentioned above with caution. All the more important is the development of an approach to constrain fire CO_2 emissions based on observations.

The greatest challenge on the path to constraints on global fire CO_2 emission estimates using satellite CO_2 observations is their low temporal sampling density. This poses a problem also for other research purposes, which has been recognised in the scientific community and subsequently, there have been some attempts to overcome this challenge. Indeed, one such attempt is the the Multi-Instrument Fused bias-corrected CO_2 Version 3 data set that I use for my work. The two observational CO_2 data sets from

OCO-2 and GOSAT were combined, which is a gain in information. However, the gaps in the individual data sets translate to the fused product, so that it is still not appropriate for medium scale studies. A similar approach was taken by Jing et al. (2014) and Wang et al. (2014), who merged GOSAT and SCIAMACHY CO_2 measurements. Various other data fusion approaches exist that aim to further enhance the CO_2 data density for both the OCO-2 as well as the GOSAT data sets using geostatistical interpolation (Liu et al. 2012; Hammerling et al. 2012; Tadić et al. 2015; Watanabe et al. 2015; Zeng et al. 2017; Chevallier et al. 2017; Zammit-Mangion et al. 2018). Particularly noteworthy is the work of Bhattacharjee et al. (2020), who combined land use and land cover (LULC) information and two auxiliary emission estimates (the Open-source Data Inventory for Anthropogenic CO_2 and the Emissions Database for Global Atmospheric Research) separately to regionally model missing CO_2 values for the OCO-2 data set. They quantified the terrestrial distribution of LULC and their impacts on local CO_2 patterns and inserted them with each of the auxiliary emission data sets into a co-kriging approach. Prediction errors with this multivariate kriging method were lower than for the baseline alternatives using univariate kriging. Another distinct advantage of this approach is its ability to model high-emission hotspots outside the OCO-2 swath. This study highlights the potential of multivariate co-kriging methods for CO_2 predictions. Recently, Jin et al. (2022) published a novel global ensemble CO_2 data set with 3-hourly resolution, covering the period from 2003 to 2020. They smoothed GOSAT-1/-2, SCIAMACHY, OCO-2/3, and TanSat data with a 30-day time window, filled missing values according to the Total Carbon Column Observing Network (TCCON) data, and merged the satellite data sets applying maximum likelihood estimation and optimal interpolation methods. The validation resulted in high correlations with the TCCON and the World Data Centre for Greenhouse Gases data sets (r=0.96, RMSE=2.62 ppm and r=0.82, RMSE=6.75 ppm, respectively). This data set provides a great opportunity for future carbon cycle studies, yet I consider the RMSE values still too high for fire emission research. With the emergence of data sets that globally map CO_2 values at a high temporal resolution, satellite-based fire emission estimates may become more realistic. However, accurately and precisely estimating CO_2 values where observations are missing remains a major issue. (Byrne et al. 2022, preprint, currently under review), who tested the suitability of OCO-2 data for simulating country-specific terrestrial carbon stock changes, conclude that improvements to atmospheric CO_2 inversion systems—as well as ground-based and aircraft-based CO_2 measurements—will be crucial to ameliorate top-down CO_2 budgets. In addition to inverse modelling, gap-filling algorithms could play an important role in the future. Yet these approaches blur the boundary between model estimates and measurement-based estimates, since part

of the measurements will be derived based on a number of assumptions. Therefore, the two methods may be complementing, but they cannot be clearly contrasted.

Previous case studies provide evidence that satellite-derived CO_2 emissions can be attributed to fires on the local scale with the support of sophisticated atmospheric transport and inversion models. Similarly, global fire emission estimates exist, and satellite-based CO_2 observations reproduce the features of ground-based CO_2 observations for the global scale very well, such as the positive trend and the seasonal fluctuations (Crowell et al. 2019). Thus, CO_2 emissions in relation to fires can be examined on the local as well as the global level. However, for the intermediate scales in between, ranging from the regional to the continental to the hemispheric scale, this does not apply. At the intermediate scales, data availability is insufficient and their accuracy is too low for fire CO_2 emission and attribution research. Closing this gap would greatly improve the branch of research. To this end, ideally in the coming years or decades more satellite missions will be launched, aiming to observe atmospheric carbon globally, especially CO_2. Even though the temporal resolution would still be rather low, this would improve data availability considerably, and broaden the basis for fused products, both of which are highly necessary to promote fire emission research.

Finally, I would like to address some important points that have been raised recently in the discussion about fires and associated greenhouse gas emissions. Stenzel et al. (2019) argue that regional fire emission models grossly overestimate emissions from US forest fires by about 60% - 80% compared to field observations, based on the misconception that the majority of the trees are burned to the ground. They propose "realistic" parameterisation of biomass combustion completeness and underline the need for accurate quantification of standing dead trees. For appropriate model results not only biomass combustion should be represented as realistically as possible, but also the area burned. As mentioned in the introduction, a substantial part of the uncertainty in fire emission inventories is due to the underlying active fire detection data, which includes fire radiative power and BA data. Unfortunately, this uncertainty cannot be eliminated with an observation-based approach, as determining active fires is also essential there. Brennan et al. (2019) estimated the theoretical uncertainties for three global remotely sensed BA products, among which is the ESA FireCCI50 data set, the predecessor of the FireCCI51 data used in this thesis. They found relative uncertainties on mean global BA of 4% - 5.5%, and emphasised that these can be higher regionally. They mount to 8% - 10% in Africa and Australia, and are larger in regions with smaller annual BA. This deficit is compounded by the non-detection of small fires, which burn only a fraction of a satellite pixel. Ramo et al. (2021) assessed the relevance

of small fires for fire carbon emissions, comparing high-resolution (20 m) multispectral instrument images from Sentinel-2 and moderate-resolution (500 m) images from MODIS. They detected 80% more BA with Sentinel-2 than with MODIS images and attribute this difference mainly to small fires. They conclude that current fire emission estimates based on MODIS data underestimate emissions by 31% - 101%. Considering that the BA product in this thesis has a coarse spatial resolution of 0.25° (28'000m at the equator), this limitation becomes even more serious.

6 Conclusion & Outlook

The goal of my Master thesis was to fathom the potential of remotely sensed carbon measurements for carbon cycle studies and CO_2 emission attribution to fires on global to local scales. This study illustrates that whether carbon data reveal a fire signal depends on the analysis method as well as on the spatial scale, and vegetation class burned, and that there are differences for CO and CO_2 observations. On the one hand there is a strong CO_2 fire signal on the Southern Hemisphere scale according to the correlation with BA, but it disintegrates with decreasing spatial scales. Time series analyses show a weak CO_2 fire signal for the two continental scales, but not for the Southern Hemisphere, nor the regional and local scales. With the FCA analysis, a carbon fire response on the global scale could not be identified. CO data reveal a strong fire signal on the local scale. In addition to CO, AOD and LST covary relatively reliably with BA on the local scale, yet there is no unambiguous sign of co-evolution on the global scale. The absence of a fire signal in the CO_2 data on the global scale and the weak evidence for fire-coupled behaviour in other parameters inhibits the development of a multivariate gap-filling algorithm building on this work. Only if CO_2 data density can be enhanced, a global fire signal is then detectable, and co-evolutions of auxiliary variables can be identified, the potential of a gap-filling approach could be tested.

The BA-carbon correlations allow for further differentiation between CO_2, corrected CO_2, and CO data and the traces that fires leave in them. CO_2 and corrected CO_2 data are, naturally, closely related and so are their correlations with BA. It is evident that correcting for the vegetation signal is valuable as it increases the correlation in virtually every case. The CO_2 and the CO data both demonstrate seasonal fluctuations. The seasonal fluctuations in the CO_2 data are generally consistent with the seasonal BA distribution, i.e. the maximum values occur simultaneously. This is not necessarily the case for seasonal CO fluctuations on the hemispherical scale, which indicates that

fires in certain regions and vegetation classes have a greater impact on atmospheric CO levels than fires in other regions. When comparing CO_2 and CO data, it appears that CO_2-BA correlations are mainly a function of the spatial scale, while CO-BA correlations seem to be driven primarily by BA per vegetation class, and only secondarily by the spatial scale. They are higher than CO_2-BA correlations for the two medium spatial scales, i.e. the larger Australian region and Australia. CO_2 and CO observations are affected differently by BA in vegetation class, which is further illustrated by conflicting maximum and minimum correlation values.

If my analyses were to be repeated I would suggest the following refinements. The analyses of fire-dependent variable behaviour would benefit greatly from higher temporal resolution data, ideally with daily observations. If no measurements are available with this resolution, temporal interpolation methods such as downsampling might be applied and the set of auxiliary parameters augmented. Experimenting with time-lagged analyses could also prove successful, as peaks in CO, AOD, and LST did not always occur at the same time as the fire peak. Regarding the correlation analyses, a global scale BA-carbon correlation could be interesting, to see if it yields similarly good results as the hemispherical correlation. If there was a way to not only correct CO_2 data for the vegetation signal, but also in a reliable form for other influences, the fire signal in the data might be further enhanced. Correction of the anthropogenic signal should take priority, followed by corrections of the volcanic and lastly the LULCC signal. Moreover, it would be interesting to see how the analyses of the Multi-Instrument Fused bias-corrected XCO_2 product compare to those of other products, e.g. to the one described by Jin et al. (2022). As this product covers the period from January 2003 to August 2020, it is moreover suitable for studying the IAV of CO_2, which is a highly relevant topic, especially in relation to fire emissions. It would be exciting to compare the IAV of CO_2 to that of BA and CO. Specifically, it would be interesting to find out if the patterns in Southern Hemisphere IAV of CO as identified by Edwards et al. (2006) are also present in the IAV of CO_2.

Both, CO_2 and CO satellite measurements feature different deficits. Constraining CO_2 emissions from fire through remote sensing observations thus remains a challenge, also for the intermediate spatial scales between the local and global scales. This is particularly revealing because the remote sensing products were specifically designed for observations at these scales. The biggest hurdle to overcome in the process towards observational constraints on fire CO_2 emissions is the lack of accurate global CO_2 observation estimates. However, there are ambitious aspirations for future developments in this direction. Most prominently, ESA and EUMETSAT are currently devel-

oping six Sentinel expansion missions, one of which is the Copernicus Anthropogenic Carbon Dioxide Monitoring (CO2M) mission. CO2M is planned as a two-satellite mission, with the option of a third satellite, and focuses on monitoring anthropogenic CO_2 emissions. The three satellites are expected to supply global observations within two to three days by 2026 (Janssens-Maenhout et al. 2020). An American nonprofit public-private partnership called "Carbon Mapper" also pursues the goal of providing more complete, timely, and precise CO_2 satellite observation in launching a multi-satellite constellation in 2025 (Schingler 2022). With such additional satellite missions and improved retrieval algorithms the availability of accurate CO_2 data will rise. This offers a great opportunity for fire emission research and increases the chances for a solid observation-based emission estimation on different spatial scales.

7 Data Availability

Most data sets used in this thesis are freely available online. L-VOD (Wigneron et al. 2021) and GRACED data (Dou et al. 2021) were kindly made available by the authors upon request. XCO_2 data is distributed via the Goddard Earth Sciences Data and Information Distribution Center (GES DISC, Nguyen et al. 2022). CO data is available via the same platform (AIRS project 2019). BA data can be obtained e.g. via the UK Centre for Environmental Data Analysis (CEDA, Chuvieco et al. 2018). NASA distributes AOD data and other CERES products online at https://ceres.larc.nasa.gov/data/. LST is also provided by NASA via the Land Processes Distributed Active Archive Center LP DAAC (Wan et al. 2015), and TWS data can be retrieved via Physical Oceanography Distributed Active Archive Center (PO DAAC, Wiese et al. 2019). NDVI data can also be obtained via NASA's LP DAAC (Didan 2021). NBP data from the TRENDY project is available at https://blogs.exeter.ac.uk/trendy/protocol/.

Acknowledgements

I am extremely grateful to Prof. Sonia Seneviratne, who welcomed me in the Land-Climate Dynamics research group and, as co-supervisor, encouraged my thesis from the beginning. Furthermore, I would like to extend my sincere thanks to my supervisor, Prof. Olivia Romppainen-Martius, who supported this work with her professional advice and facilitated the cooperation with the Institute for Atmospheric and Climate Science at ETH Zürich. I am also very thankful to Prof. Stefan Brönnimann, who was willing to chair my Master's examination.

This endeavour would not have been possible without the constant support of Verena Bessenbacher. I would like to express my deepest appreciation for her invaluable patience and the inspiring discussions. She always gave me great guidance without restricting my scientific freedom. Working with her was not only very pleasant on the professional, but also on the personal level.

Thanks should also go to Dr. Lukas Gudmundsson and Dr. Laibao Liu for their interest in this thesis and their repeated constructive feedback. I am grateful to the whole Land-Climate Dynamics research team: it was an honour and a pleasure to work with people so motivated and motivating.

I would also like to thank the international research community and experts in the field of fire CO_2 emissions for sharing their data, for their encouraging comments on my work, and for the wealth of knowledge that I could draw on.

Finally, I would like to thank my family, especially my parents, and friends. Without them I would not be where and who I am today.

References

Adkins, Jaron, Jonathan Sanderman and Jessica Miesel (2019). 'Soil carbon pools and fluxes vary across a burn severity gradient three years after wildfire in Sierra Nevada mixed-conifer forest'. In: *Geoderma* 333, pp. 10–22. ISSN: 0016-7061. DOI: 10.1016/j.geoderma.2018.07.009.

AIRS project (2019). *Aqua/AIRS L3 Monthly Standard Physical Retrieval (AIRS-only) 1 degree x 1 degree V7.0*. Greenbelt, MD, USA, Goddard Earth Sciences Data and Information Services Center (GES DISC), Accessed: 2022-01-26. DOI: 10.5067/UBENJB9D3T2H.

Andreae, M. O. et al. (2012). 'Carbon monoxide and related trace gases and aerosols over the Amazon Basin during the wet and dry seasons'. In: *Atmospheric Chemistry and Physics* 12.13. Publisher: Copernicus GmbH, pp. 6041–6065. ISSN: 1680-7316. DOI: 10.5194/acp-12-6041-2012.

Archibald, S. et al. (2018). 'Biological and geophysical feedbacks with fire in the Earth system'. In: *Environmental Research Letters* 13.3. Publisher: IOP Publishing, p. 033003. ISSN: 1748-9326. DOI: 10.1088/1748-9326/aa9ead.

Bacastow, R. B., C. D. Keeling and T. P. Whorf (1985). 'Seasonal amplitude increase in atmospheric CO2 concentration at Mauna Loa, Hawaii, 1959–1982'. In: *Journal of Geophysical Research: Atmospheres* 90.D6, pp. 10529–10540. ISSN: 2156-2202. DOI: 10.1029/JD090iD06p10529.

Badr, O. and S. D. Probert (1995). 'Sinks and environmental impacts for atmospheric carbon monoxide'. In: *Applied Energy* 50.4, pp. 339–372. ISSN: 0306-2619. DOI: 10.1016/0306-2619(95)98803-A.

Ballantyne, Ashley et al. (2012). 'Increase in observed net carbon dioxide uptake by land and oceans during the past 50 years'. In: *Nature* 488. DOI: 10.1038/nature11299.

Batllori, Enric et al. (2018). 'Compound fire-drought regimes promote ecosystem transitions in Mediterranean ecosystems'. In: *Journal of Ecology* 107.3, pp. 1187–1198. ISSN: 1365-2745. DOI: 10.1111/1365-2745.13115.

Bhattacharjee, Shrutilipi and Jia Chen (2020). 'Prediction of Satellite-Based Column CO_2 Concentration by Combining Emission Inventory and LULC Information'. In: *IEEE Transactions on Geoscience and Remote Sensing*, pp. 1–16. DOI: 10.1109/TGRS.2020.2985047.

Bistinas, I. et al. (2014). 'Causal relationships versus emergent patterns in the global controls of fire frequency'. In: *Biogeosciences* 11.18, pp. 5087–5101. DOI: 10.5194/bg-11-5087-2014.

Blackhall, Melisa et al. (2017). 'Effects of biological legacies and herbivory on fuels and flammability traits: A long-term experimental study of alternative stable states'. In:

Journal of Ecology 105.5, pp. 1309–1322. ISSN: 1365-2745. DOI: 10.1111/1365-2745.12796.

Bond, William J., F. I. Woodward and G. F. Midgley (2004). 'The global distribution of ecosystems in a world without fire - Bond - 2005 - New Phytologist - Wiley Online Library'. In: *New Phytologist* 165, pp. 525–537. DOI: https://doi.org/10.1111/j.1469-8137.2004.01252.x.

Brando, Paulo M. et al. (2019). 'Droughts, Wildfires, and Forest Carbon Cycling: A Pantropical Synthesis'. In: *Annual Review of Earth and Planetary Sciences* 47.1. DOI: 10.1146/annurev-earth-082517-010235.

Brennan, James et al. (2019). 'Theoretical uncertainties for global satellite-derived burned area estimates'. In: *Biogeosciences* 16.16. Publisher: Copernicus GmbH, pp. 3147–3164. ISSN: 1726-4170. DOI: 10.5194/bg-16-3147-2019.

Burton, Chantelle et al. (2020). 'El Niño Driven Changes in Global Fire 2015/16'. In: *Frontiers in Earth Science* 8. ISSN: 2296-6463.

Byrne, B. et al. (2021). 'The Carbon Cycle of Southeast Australia During 2019–2020: Drought, Fires, and Subsequent Recovery'. In: *AGU Advances* 2.4. ISSN: 2576-604X. DOI: 10.1029/2021AV000469.

Byrne, Brendan et al. (2022). 'National CO_2 budgets (2015–2020) inferred from atmospheric CO_2 observations in support of the Global Stocktake'. In: *Earth System Science Data Discussions*. Publisher: Copernicus GmbH, pp. 1–59. ISSN: 1866-3508. DOI: 10.5194/essd-2022-213.

Cardil, Adrián et al. (2021). 'Coupled effects of climate teleconnections on drought, Santa Ana winds and wildfires in southern California'. In: *Science of The Total Environment* 765, p. 142788. ISSN: 0048-9697. DOI: 10.1016/j.scitotenv.2020.142788.

Cheng, Y. et al. (2013). 'Biomass burning contribution to Beijing aerosol'. In: *Atmospheric Chemistry and Physics* 13.15. Publisher: Copernicus GmbH, pp. 7765–7781. ISSN: 1680-7316. DOI: 10.5194/acp-13-7765-2013.

Chevallier, Frédéric et al. (2017). 'Probabilistic global maps of the CO2 column at daily and monthly scales from sparse satellite measurements'. In: *Journal of Geophysical Research: Atmospheres* 122.14, pp. 7614–7629. ISSN: 2169-8996. DOI: 10.1002/2017JD026453.

Chuvieco, Emilio et al. (2018). *ESA CCI ECV Fire Disturbance: D4.2 Product User Guide*. ESA Fire Climate Change Initiative (Fire_cci): MODIS Fire_cci Burned Area Pixel product, version 5.1. Centre for Environmental Data Analysis, DOI: 10.5285/58f00d8814064b79a0c49662ad3af53

Ciais, P. et al. (2013). *Carbon and Other Biogeochemical Cycles*. Cambridge, United Kingdom and New York, NY, USA: Cambridge University Press.

Ciais, P. et al. (2019). 'Five decades of northern land carbon uptake revealed by the interhemispheric CO2 gradient'. In: *Nature* 568.7751, pp. 221–225. ISSN: 0028-0836, 1476-4687. DOI: 10.1038/s41586-019-1078-6.

Connor, Brian et al. (2016). 'Quantification of uncertainties in OCO-2 measurements of XCO_2: simulations and linear error analysis'. In: *Atmospheric Measurement Techniques* 9.10. Publisher: Copernicus GmbH, pp. 5227–5238. ISSN: 1867-1381. DOI: 10.5194/amt-9-5227-2016.

Connor, Brian J. et al. (2008). 'Orbiting Carbon Observatory: Inverse method and prospective error analysis'. In: *Journal of Geophysical Research: Atmospheres* 113.D5. ISSN: 2156-2202. DOI: 10.1029/2006JD008336.

Crowell, Sean et al. (2019). 'The 2015–2016 carbon cycle as seen from OCO-2 and the global in situ network'. In: *Atmospheric Chemistry and Physics* 19.15. Publisher: Copernicus GmbH, pp. 9797–9831. ISSN: 1680-7316. DOI: 10.5194/acp-19-9797-2019.

Csiszar, I.A., J.T. Morisette and L. Giglio (2006). 'Validation of active fire detection from moderate-resolution satellite sensors: the MODIS example in northern eurasia'. In: *IEEE Transactions on Geoscience and Remote Sensing* 44.7. Conference Name: IEEE Transactions on Geoscience and Remote Sensing, pp. 1757–1764. ISSN: 1558-0644. DOI: 10.1109/TGRS.2006.875941.

Darmenov, Anton and Arlindo da Silva (2013). 'The quick fire emissions dataset (QFED): Documentation of versions 2.1, 2.2 and 2.4'. In: *NASA Technical Report Series on Global Modeling and Data Assimilation, NASA TM-2013-104606* 32, p. 183.

Davis, Kimberley T., Philip E. Higuera and Anna Sala (2018). 'Anticipating fire-mediated impacts of climate change using a demographic framework'. In: *Functional Ecology* 32.7, pp. 1729–1745. ISSN: 1365-2435. DOI: 10.1111/1365-2435.13132.

Didan, Kamel (2021). *ESA CCI ECV Fire Disturbance: D4.2 Product User Guide*. MODIS/Terra Vegetation Indices Monthly L3 Global 0.05Deg CMG V061 [Data set]. NASA EOSDIS Land Processes DAAC. DOI: doi.org/10.5067/MODIS/MOD13C2.061.

Dou, Xinyu et al. (2021). 'Near-real-time global gridded daily CO2 emissions'. In: *The Innovation* 3.1, p. 100182. ISSN: 2666-6758. DOI: 10.1016/j.xinn.2021.100182.

Edwards, D. P. et al. (2006). 'Southern Hemisphere carbon monoxide interannual variability observed by Terra/Measurement of Pollution in the Troposphere (MOPITT)'. In: *Journal of Geophysical Research: Atmospheres* 111.D16. ISSN: 2156-2202. DOI: 10.1029/2006JD007079.

ESA (2017). *Land Cover CCI Product User Guide Version 2*. Version 2. Available at. URL: maps.elie.ucl.ac.be/CCI/viewer/download/ESACCI-LC-Ph2-PUGv2_2.0.pdf.

– (2022). *GOSAT Objectives - Earth Online*. URL: https://earth.esa.int/eogateway/missions/gosat/objectives (visited on 11/10/2022).

Fernandez-Moran, R. et al. (2017). 'A new calibration of the effective scattering albedo and soil roughness parameters in the SMOS SM retrieval algorithm'. In: *International Journal of Applied Earth Observation and Geoinformation* 62, pp. 27–38. ISSN: 1569-8432. DOI: 10.1016/j.jag.2017.05.013.

Field, R. D. et al. (2015). 'Development of a Global Fire Weather Database'. In: *Natural Hazards and Earth System Sciences* 15.6. Publisher: Copernicus GmbH, pp. 1407–1423. ISSN: 1561-8633. DOI: 10.5194/nhess-15-1407-2015.

Fillmore, David W. et al. (2022). 'Evaluation of aerosol optical depths and clear-sky radiative fluxes of the CERES Edition 4.1 SYN1deg data product'. In: *Atmospheric Chemistry and Physics* 22.15, pp. 10115–10137. ISSN: 1680-7324. DOI: 10.5194/acp-22-10115-2022.

Fischer, E. M., S. Sippel and R. Knutti (2021). 'Increasing probability of record-shattering climate extremes'. In: *Nature Climate Change* 11.8. Number: 8 Publisher: Nature Publishing Group, pp. 689–695. ISSN: 1758-6798. DOI: 10.1038/s41558-021-01092-9.

Fischer, E. M. et al. (2007). 'European climate response to tropical volcanic eruptions over the last half millennium'. In: *Geophysical Research Letters* 34.5. ISSN: 1944-8007. DOI: 10.1029/2006GL027992.

Fischer, Tobias P. and Alessandro Aiuppa (2020). 'AGU Centennial Grand Challenge: Volcanoes and Deep Carbon Global CO2 Emissions From Subaerial Volcanism—Recent Progress and Future Challenges'. In: *Geochemistry, Geophysics, Geosystems* 21.3. ISSN: 1525-2027. DOI: 10.1029/2019GC008690.

Forkel, Matthias et al. (2017). 'A data-driven approach to identify controls on global fire activity from satellite and climate observations (SOFIA V1)'. In: *Geoscientific Model Development* 10.12. Publisher: Copernicus GmbH, pp. 4443–4476. ISSN: 1991-959X. DOI: 10.5194/gmd-10-4443-2017.

Friedlingstein, Pierre et al. (2020). 'Global Carbon Budget 2020'. In: *Earth System Science Data* 12.4. Publisher: Copernicus GmbH, pp. 3269–3340. ISSN: 1866-3508. DOI: 10.5194/essd-12-3269-2020.

Friedlingstein, Pierre et al. (2021). 'Global Carbon Budget 2021'. In: *Earth System Science Data Discussions*. Publisher: Copernicus GmbH, pp. 1–191. ISSN: 1866-3508. DOI: 10.5194/essd-2021-386.

Fuller, Douglas O. and Kevin Murphy (2006). 'The Enso-Fire Dynamic in Insular Southeast Asia'. In: *Climatic Change* 74.4, pp. 435–455. ISSN: 1573-1480. DOI: 10.1007/s10584-006-0432-5.

Garcia, Mariano et al. (2017). 'Quantifying biomass consumption and carbon release from the California Rim fire by integrating airborne LiDAR and Landsat OLI data'. In:

Journal of Geophysical Research: Biogeosciences 122.2, pp. 340–353. ISSN: 2169-8961. DOI: 10.1002/2015JG003315.

Grassi, Giacomo et al. (2017). 'The key role of forests in meeting climate targets requires science for credible mitigation'. In: *Nature Climate Change* 7.3. Number: 3 Publisher: Nature Publishing Group, pp. 220–226. ISSN: 1758-6798. DOI: 10.1038/nclimate3227.

Guo, Meng et al. (2017). 'CO2 emissions from the 2010 Russian wildfires using GOSAT data'. In: *Environmental Pollution* 226, pp. 60–68. ISSN: 0269-7491. DOI: 10.1016/j.envpol.2017.04.014.

Guo, Meng et al. (2019). 'Estimation of CO2 Emissions from Wildfires Using OCO-2 Data'. In: *Atmosphere* 10.10. Number: 10 Publisher: Multidisciplinary Digital Publishing Institute, p. 581. ISSN: 2073-4433. DOI: 10.3390/atmos10100581.

Gutknecht, Jessica L. M., Hugh A. L. Henry and Teri C. Balser (2010). 'Inter-annual variation in soil extra-cellular enzyme activity in response to simulated global change and fire disturbance'. In: *Pedobiologia* 53.5, pp. 283–293. ISSN: 0031-4056. DOI: 10.1016/j.pedobi.2010.02.001.

Hammerling, Dorit and Anna Michalak (2012). 'Mapping of CO2 at high spatiotemporal resolution using satellite observations: Global distributions from OCO-2'. In: *Journal of Geophysical Research (Atmospheres)* 117, p. 6306. DOI: 10.1029/2011JD017015.

Harrison, S. P. et al. (2018). 'The biomass burning contribution to climate–carbon-cycle feedback'. In: *Earth System Dynamics* 9.2, pp. 663–677. DOI: 10.5194/esd-9-663-2018.

He, Tianhua and Byron B Lamont (2018). 'Baptism by fire: the pivotal role of ancient conflagrations in evolution of the Earth's flora'. In: *National Science Review* 5.2, pp. 237–254. ISSN: 2095-5138. DOI: 10.1093/nsr/nwx041.

Hessl, Amy E., Don McKenzie and Richard Schellhaas (2004). 'Drought and Pacific Decadal Oscillation Linked to Fire Occurrence in the Inland Pacific Northwest'. In: *Ecological Applications* 14.2, pp. 425–442. ISSN: 1939-5582. DOI: 10.1890/03-5019.

Heymann, J. et al. (2017). 'CO 2 emission of Indonesian fires in 2015 estimated from satellite-derived atmospheric CO 2 concentrations: 2015 Indonesian fire CO2 emission'. In: *Geophysical Research Letters* 44. DOI: 10.1002/2016GL072042.

Humphrey, Vincent et al. (2018). 'Sensitivity of atmospheric CO2 growth rate to observed changes in terrestrial water storage'. In: *Nature* 560. DOI: 10.1038/s41586-018-0424-4.

Hurteau, Matthew D. and Matthew L. Brooks (2011). 'Short- and Long-term Effects of Fire on Carbon in US Dry Temperate Forest Systems'. In: *BioScience* 61.2, pp. 139–146. ISSN: 0006-3568. DOI: 10.1525/bio.2011.61.2.9.

Ichoku, C. and L. Ellison (2014). 'Global top-down smoke-aerosol emissions estimation using satellite fire radiative power measurements'. In: *Atmospheric Chemistry and*

Physics 14.13. Publisher: Copernicus GmbH, pp. 6643–6667. ISSN: 1680-7316. DOI: 10.5194/acp-14-6643-2014.

Inoue, M. et al. (2013). 'Validation of XCO_2 derived from SWIR spectra of GOSAT TANSO-FTS with aircraft measurement data'. In: *Atmospheric Chemistry and Physics* 13.19. Publisher: Copernicus GmbH, pp. 9771–9788. ISSN: 1680-7316. DOI: 10.5194/acp-13-9771-2013.

IPCC (2021). 'Summary for Policymakers'. In: *Climate Change 2021: The Physical Science Basis. Contribution of Working Group I to the Sixth Assessment Report of the Intergovernmental Panel on Climate Change*, pp. 3–32. DOI: 10.1017/9781009157896.001.

Iturbide, Maialen et al. (2020). 'An update of IPCC climate reference regions for subcontinental analysis of climate model data: definition and aggregated datasets'. In: *Earth System Science Data* 12.4. Publisher: Copernicus GmbH, pp. 2959–2970. ISSN: 1866-3508. DOI: 10.5194/essd-12-2959-2020.

Janardanan, Rajesh et al. (2016). 'Comparing GOSAT observations of localized CO_2 enhancements by large emitters with inventory-based estimates'. In: *Geophysical Research Letters* 43.7, pp. 3486–3493. ISSN: 0094-8276, 1944-8007. DOI: 10.1002/2016GL067843.

Janssens-Maenhout, G. et al. (2020). 'Toward an Operational Anthropogenic CO2 Emissions Monitoring and Verification Support Capacity'. In: *Bulletin of the American Meteorological Society* 101.8. Publisher: American Meteorological Society Section: Bulletin of the American Meteorological Society, E1439–E1451. ISSN: 0003-0007, 1520-0477. DOI: 10.1175/BAMS-D-19-0017.1.

Jia, Gensuo et al. (2019). 'Climate Change and Land: an IPCC special report on climate change, desertification, land degradation, sustainable land management, food security, and greenhouse gas fluxes in terrestrial ecosystems'. In: pp. 131–247.

Jin, Chunlin et al. (2022). 'A long-term global XCO2 dataset: Ensemble of satellite products'. In: *Atmospheric Research* 279, p. 106385. ISSN: 01698095. DOI: 10.1016/j.atmosres.2022.106385.

Jing, Yingying et al. (2014). 'Mapping Global Atmospheric CO2 Concentration at High Spatiotemporal Resolution'. In: *Atmosphere* 5.4. Number: 4 Publisher: Multidisciplinary Digital Publishing Institute, pp. 870–888. ISSN: 2073-4433. DOI: 10.3390/atmos5040870.

Johnstone, Jill F et al. (2016). 'Changing disturbance regimes, ecological memory, and forest resilience'. In: *Frontiers in Ecology and the Environment* 14.7, pp. 369–378. ISSN: 1540-9295, 1540-9309. DOI: 10.1002/fee.1311.

Jolly, W. Matt et al. (2015). 'Climate-induced variations in global wildfire danger from 1979 to 2013'. In: *Nature Communications* 6.1. Number: 1 Publisher: Nature Publishing Group, p. 7537. ISSN: 2041-1723. DOI: 10.1038/ncomms8537.

Jones, Matthew W. et al. (2022). 'Global and Regional Trends and Drivers of Fire Under Climate Change'. In: *Reviews of Geophysics* 60.3, e2020RG000726. ISSN: 1944-9208. DOI: 10.1029/2020RG000726.

Kaiser, J. W. et al. (2012). 'Biomass burning emissions estimated with a global fire assimilation system based on observed fire radiative power'. In: *Biogeosciences* 9.1. Publisher: Copernicus GmbH, pp. 527–554. ISSN: 1726-4170. DOI: 10.5194/bg-9-527-2012.

Keeley, Jon E. and Philip W. Rundel (2005). 'Fire and the Miocene expansion of C4 grasslands'. In: *Ecology Letters* 8.7, pp. 683–690. ISSN: 1461-0248. DOI: 10.1111/j.1461-0248.2005.00767.x.

Kelley, Douglas I. et al. (2019). 'How contemporary bioclimatic and human controls change global fire regimes'. In: *Nature Climate Change* 9.9. Number: 9 Publisher: Nature Publishing Group, pp. 690–696. ISSN: 1758-6798. DOI: 10.1038/s41558-019-0540-7.

Khalil, M. A. K. and R. A. Rasmussen (1990). 'The global cycle of carbon monoxide: Trends and mass balance'. In: *Chemosphere* 20.1, pp. 227–242. ISSN: 0045-6535. DOI: 10.1016/0045-6535(90)90098-E.

Landerer, Felix W. et al. (2020). 'Extending the Global Mass Change Data Record: GRACE Follow-On Instrument and Science Data Performance'. In: *Geophysical Research Letters* 47.12, e2020GL088306. ISSN: 1944-8007. DOI: 10.1029/2020GL088306.

Langenfelds, R. L. et al. (2002). 'Interannual growth rate variations of atmospheric CO2 and its δ13C, H2, CH4, and CO between 1992 and 1999 linked to biomass burning'. In: *Global Biogeochemical Cycles* 16.3. ISSN: 1944-9224. DOI: 10.1029/2001GB001466.

Lasslop, Gitta et al. (2019). 'Influence of Fire on the Carbon Cycle and Climate'. In: *Current Climate Change Reports* 5.2, pp. 112–123. ISSN: 2198-6061. DOI: 10.1007/s40641-019-00128-9.

Lesk, Corey, Pedram Rowhani and Navin Ramankutty (2016). 'Influence of extreme weather disasters on global crop production'. In: *Nature* 529.7584. Number: 7584 Publisher: Nature Publishing Group, pp. 84–87. ISSN: 1476-4687. DOI: 10.1038/nature16467.

Li, Andy X., Yuan Wang and Yuk L. Yung (2019). 'Inducing Factors and Impacts of the October 2017 California Wildfires'. In: *Earth and Space Science* 6.8, pp. 1480–1488. ISSN: 2333-5084. DOI: 10.1029/2019EA000661.

Li, Xiaojun et al. (2020a). 'Compared performances of SMOS-IC soil moisture and vegetation optical depth retrievals based on Tau-Omega and Two-Stream microwave emission models'. In: *Remote Sensing of Environment* 236, p. 111502. ISSN: 0034-4257. DOI: 10.1016/j.rse.2019.111502.

Li, Xiaojun et al. (2020b). 'Development and Validation of the SMOS-IC Version 2 (V2) Soil Moisture Product'. In: *IGARSS 2020 - 2020 IEEE International Geoscience and Remote Sensing Symposium*. ISSN: 2153-7003, pp. 4434–4437. DOI: 10.1109/IGARSS39084.2020.9323324.

Li, Xiaojun et al. (2021). 'Global-scale assessment and inter-comparison of recently developed/reprocessed microwave satellite vegetation optical depth products'. In: *Remote Sensing of Environment* 253, p. 112208. ISSN: 0034-4257. DOI: 10.1016/j.rse.2020.112208.

Lin, Yuh-Lang (2007). *Mesoscale Dynamics*. Cambridge University Press, p. 1. DOI: 10.1017/CBO9780511619649.

Liu, Junjie et al. (2017). 'Contrasting carbon cycle responses of the tropical continents to the 2015–2016 El Niño'. In: *Science* 358.6360. Publisher: American Association for the Advancement of Science, eaam5690. DOI: 10.1126/science.aam5690.

Liu, Tianjia et al. (2020). 'Diagnosing spatial biases and uncertainties in global fire emissions inventories: Indonesia as regional case study'. In: *Remote Sensing of Environment* 237, p. 111557. ISSN: 0034-4257. DOI: 10.1016/j.rse.2019.111557.

Liu, Yang et al. (2012). 'Mapping the FTS SWIR L2 product of XCO $_2$ and XCH $_4$ data from the GOSAT by the Kriging method – a case study in East Asia'. In: *International Journal of Remote Sensing* 33.10, pp. 3004–3025. ISSN: 0143-1161, 1366-5901. DOI: 10.1080/01431161.2011.624132.

Liu, Zhihua, Ashley P. Ballantyne and L. Annie Cooper (2019). 'Biophysical feedback of global forest fires on surface temperature'. In: *Nature Communications* 10.1. Publisher: Nature Publishing Group, p. 214. ISSN: 2041-1723.

Lizundia-Loiola, Joshua et al. (2020). 'A spatio-temporal active-fire clustering approach for global burned area mapping at 250 m from MODIS data'. In: *Remote Sensing of Environment* 236, p. 111493. DOI: 10.1016/j.rse.2019.111493.

Mao, Jianping et al. (2021). 'Measuring Atmospheric CO2 Enhancements From the 2017 British Columbia Wildfires Using a Lidar'. In: *Geophysical Research Letters* 48.16. _eprint: https://onlinelibrary.wiley.com/doi/pdf/10.1029/2021GL093805, e2021GL093805. ISSN: 1944-8007. DOI: 10.1029/2021GL093805.

McLauchlan, Kendra K. et al. (2020). 'Fire as a fundamental ecological process: Research advances and frontiers'. In: *Journal of Ecology* 108.5, pp. 2047–2069. ISSN: 1365-2745. DOI: 10.1111/1365-2745.13403.

Miesel, Jessica R. et al. (2015). 'Soil organic matter composition and quality across fire severity gradients in coniferous and deciduous forests of the southern boreal region'. In: *Journal of Geophysical Research: Biogeosciences* 120.6, pp. 1124–1141. ISSN: 21698953. DOI: 10.1002/2015JG002959.

Moghim, Sanaz (2020). 'Assessment of Water Storage Changes Using GRACE and GLDAS'. In: *Water Resources Management* 34.2, pp. 685–697. ISSN: 1573-1650. DOI: 10.1007/s11269-019-02468-5.

NASA (2022). *Orbiting Carbon Observatory-2: Science*. URL: https://ocov2.jpl.nasa.gov/science/ (visited on 11/10/2022).

Nguyen, Hai et al. (2022). *Multi-Instrument Fused bias-corrected XCO_2 and other select fields aggregated as Level 4 daily files*. Greenbelt, MD, USA, Goddard Earth Sciences Data and Information Services Center (GES DISC), Accessed: 2021-08-30. DOI: 10.5067/ZS346LH1NTIS.

Nicolai-Shaw, Nadine et al. (2017). 'A drought event composite analysis using satellite remote-sensing based soil moisture'. In: *Remote Sensing of Environment*. Earth Observation of Essential Climate Variables 203, pp. 216–225. ISSN: 0034-4257. DOI: 10.1016/j.rse.2017.06.014.

O'Dell, C. W. et al. (2012). 'The ACOS CO_2 retrieval algorithm – Part 1: Description and validation against synthetic observations'. In: *Atmospheric Measurement Techniques* 5.1. Publisher: Copernicus GmbH, pp. 99–121. ISSN: 1867-1381. DOI: 10.5194/amt-5-99-2012.

O'Donnell, A. J. et al. (2011). 'Climatic anomalies drive wildfire occurrence and extent in semi-arid shrublands and woodlands of southwest Australia'. In: *Ecosphere* 2.11, art127. ISSN: 2150-8925. DOI: 10.1890/ES11-00189.1.

Pagano, Thomas S. and Vivienne H. Payne (2022). 'The Atmospheric Infrared Sounder'. In: *Handbook of Air Quality and Climate Change*. Ed. by Hajime Akimoto and Hiroshi Tanimoto. Singapore: Springer Singapore, pp. 1–13. ISBN: 9789811525278. DOI: 10.1007/978-981-15-2527-8_64-1.

Patra, P. K. et al. (2009). 'Transport mechanisms for synoptic, seasonal and interannual SF_6 variations and "age" of air in troposphere'. In: *Atmospheric Chemistry and Physics* 9.4. Publisher: Copernicus GmbH, pp. 1209–1225. ISSN: 1680-7316. DOI: 10.5194/acp-9-1209-2009.

Pausas, Juli G. (2015). 'Evolutionary fire ecology: lessons learned from pines'. In: *Trends in Plant Science* 20.5. Publisher: Elsevier, pp. 318–324. ISSN: 1360-1385. DOI: 10.1016/j.tplants.2015.03.001.

Pausas, Juli G., Jon E. Keeley and Dylan W. Schwilk (2017). 'Flammability as an ecological and evolutionary driver'. In: *Journal of Ecology* 105.2, pp. 289–297. ISSN: 1365-2745. DOI: 10.1111/1365-2745.12691.

Pearman, G. I. and P. Hyson (1980). 'Activities of the global biosphere as reflected in atmospheric CO2 records'. In: *Journal of Geophysical Research: Oceans* 85.C8, pp. 4457–4467. ISSN: 2156-2202. DOI: 10.1029/JC085iC08p04457.

Pereira, Gabriel et al. (2009). 'Estimating trace gas and aerosol emissions over South America: Relationship between fire radiative energy released and aerosol optical depth observations'. In: *Atmospheric Environment* 43.40, pp. 6388–6397. ISSN: 1352-2310. DOI: 10.1016/j.atmosenv.2009.09.013.

Pettinari, Maria Lucrecia, Joshua Lizundia-Loiola and Emilio Chuvieco (2020). *ESA CCI ECV Fire Disturbance: D4.2 Product User Guide*. - MODIS, version 1.0. Available at. URL: https://www.esa-fire-cci.org/documents.

Pettorelli, Nathalie et al. (2005). 'Using the satellite-derived NDVI to assess ecological responses to environmental change'. In: *Trends in Ecology & Evolution* 20.9, pp. 503–510. ISSN: 0169-5347. DOI: 10.1016/j.tree.2005.05.011.

Pongratz, Julia et al. (2021). 'Land Use Effects on Climate: Current State, Recent Progress, and Emerging Topics'. In: *Current Climate Change Reports* 7.4, pp. 99–120. ISSN: 2198-6061. DOI: 10.1007/s40641-021-00178-y.

Ramillien, G., J. S. Famiglietti and J. Wahr (2008). 'Detection of Continental Hydrology and Glaciology Signals from GRACE: A Review'. In: *Surveys in Geophysics* 29.4, pp. 361–374. ISSN: 1573-0956. DOI: 10.1007/s10712-008-9048-9.

Ramo, Ruben et al. (2021). 'African burned area and fire carbon emissions are strongly impacted by small fires undetected by coarse resolution satellite data'. In: *Proceedings of the National Academy of Sciences* 118.9, e2011160118. ISSN: 0027-8424, 1091-6490. DOI: 10.1073/pnas.2011160118.

Randerson, J. T. et al. (2006). 'The Impact of Boreal Forest Fire on Climate Warming'. In: *Science* 314.5802. Publisher: American Association for the Advancement of Science, pp. 1130–1132. DOI: 10.1126/science.1132075.

Randerson, J. T. et al. (2018). *Global Fire Emissions Database, Version 4, (GFEDv4)*. Oak Ridge, Tennessee, USA: ORNL DAAC. DOI: https://doi.org/10.3334/ORNLDAAC/1293.

Rao, Mukund P. et al. (2019). 'A double bootstrap approach to Superposed Epoch Analysis to evaluate response uncertainty'. In: *Dendrochronologia* 55, pp. 119–124. ISSN: 1125-7865. DOI: 10.1016/j.dendro.2019.05.001.

Reid, J. S. et al. (2012). 'Multi-scale meteorological conceptual analysis of observed active fire hotspot activity and smoke optical depth in the Maritime Continent'. In: *Atmospheric Chemistry and Physics* 12.4. Publisher: Copernicus GmbH, pp. 2117–2147. ISSN: 1680-7316. DOI: 10.5194/acp-12-2117-2012.

Rohli, Robert and Anthony Vega (2015). *Climatology*. Third edition. Jones & Bartlett learning titles in physical science. Burlington, MA: Jones & Bartlett Learning, p. 5. ISBN: 9781284028775.

Rooney, Brigitte et al. (2020). 'Air quality impact of the Northern California Camp Fire of November 2018'. In: *Atmospheric Chemistry and Physics* 20.23. Publisher: Copernicus GmbH, pp. 14597–14616. ISSN: 1680-7316. DOI: 10.5194/acp-20-14597-2020.

Saha, Michael V., Paolo D'Odorico and Todd M. Scanlon (2017). 'Albedo changes after fire as an explanation of fire-induced rainfall suppression'. In: *Geophysical Research Letters* 44.8, pp. 3916–3923. ISSN: 1944-8007. DOI: 10.1002/2017GL073623.

Schingler, Robbie (2022). *Carbon Mapper launches Satellite Program to pinpoint Methane and CO2 Super Emitters*. URL: https://www.planet.com/pulse/carbon-mapper-launches-satellite-program-to-pinpoint-methane-and-co2-super-emitters/ (visited on 04/10/2022).

Schwandner, Florian M. et al. (2017). 'Spaceborne detection of localized carbon dioxide sources'. In: *Science* 358.6360, eaam5782. DOI: 10.1126/science.aam5782.

Seiler, Wolfgang (1974). 'The cycle of atmospheric CO'. In: *Tellus* 26.1-2, pp. 116–135. ISSN: 00402826, 21533490. DOI: 10.1111/j.2153-3490.1974.tb01958.x.

Seinfeld, John H. and Spyros N. Pandis (2016). *Atmospheric chemistry and physics : from air pollution to climate change*. Third edition. Hoboken, New Jersey: Wiley, p. 18. ISBN: 1118947401.

Shinozuka, Yohei et al. (2007). 'Aircraft profiles of aerosol microphysics and optical properties over North America: Aerosol optical depth and its association with PM2.5 and water uptake'. In: *Journal of Geophysical Research: Atmospheres* 112.D12. ISSN: 2156-2202. DOI: 10.1029/2006JD007918.

Shiraishi, Tomohiro and Ryuichi Hirata (2021). 'Estimation of carbon dioxide emissions from the megafires of Australia in 2019–2020'. In: *Scientific Reports* 11.1. Number: 1 Publisher: Nature Publishing Group, p. 8267. ISSN: 2045-2322. DOI: 10.1038/s41598-021-87721-x.

Sitch, Stephen et al. (2015). 'Recent trends and drivers of regional sources and sinks of carbon dioxide'. In: *Biogeosciences* 12. DOI: 10.5194/bg-12-653-2015.

Skinner, Carl N. et al. (2008). 'Influences of climate on fire regimes in montane forests of north-western Mexico'. In: *Journal of Biogeography* 35.8, pp. 1436–1451. ISSN: 1365-2699. DOI: 10.1111/j.1365-2699.2008.01893.x.

Stenzel, Jeffrey E. et al. (2019). 'Fixing a snag in carbon emissions estimates from wildfires'. In: *Global Change Biology* 25.11, pp. 3985–3994. ISSN: 1354-1013, 1365-2486. DOI: 10.1111/gcb.14716.

Suji, K. J. and P. R. Prince (2018). 'Superposed Epoch Analysis of High Latitude Ionospheric Joule Heating during Major Geomagnetic Storms over three Solar Cycles'. In: *Proceedings of the International Astronomical Union* 13.S340. Publisher: Cambridge University Press, pp. 67–68. ISSN: 1743-9213, 1743-9221. DOI: 10.1017/S1743921318001941.

Tadić, J. M. et al. (2015). 'Mapping of satellite Earth observations using moving window block kriging'. In: *Geoscientific Model Development* 8.10. Publisher: Copernicus GmbH, pp. 3311–3319. ISSN: 1991-959X. DOI: 10.5194/gmd-8-3311-2015.

Tang, Rongyun et al. (2021). 'Interannual variability and climatic sensitivity of global wildfire activity'. In: *Advances in Climate Change Research* 12.5, pp. 686–695. ISSN: 1674-9278. DOI: 10.1016/j.accre.2021.07.001.

Tapley, B. D. et al. (2004). 'The gravity recovery and climate experiment: Mission overview and early results'. In: *Geophysical Research Letters* 31.9. ISSN: 1944-8007. DOI: 10.1029/2004GL019920.

Tian, Baijun et al. (2020). 'AIRS Version 7 Level 3 Product User Guide'. In: p. 34.

van der Velde, Ivar R. et al. (2021). 'Vast CO2 release from Australian fires in 2019–2020 constrained by satellite'. In: *Nature* 597.7876. Publisher: Nature Publishing Group, pp. 366–369. ISSN: 1476-4687. DOI: 10.1038/s41586-021-03712-y.

Wan, Zhengming, Simon Hook and Glynn Hulley (2015). *MOD11C1 MODIS/Terra Land Surface Temperature/Emissivity Daily L3 Global 0.05Deg CMG V006 [Data set]*. NASA EOSDIS Land Processes DAAC. Accessed: 2021-09-20. DOI: 10.5067/MODIS/MOD11C1.006.

Wang, Jun et al. (2020). 'Spaceborne detection of XCO_2 enhancement induced by Australian mega-bushfires'. In: *Environmental Research Letters* 15.12. Publisher: IOP Publishing, p. 124069. ISSN: 1748-9326. DOI: 10.1088/1748-9326/abc846.

Wang, Tianxing et al. (2014). 'Combining XCO2 Measurements Derived from SCIAMACHY and GOSAT for Potentially Generating Global CO2 Maps with High Spatiotemporal Resolution'. In: *PLOS ONE* 9.8. Publisher: Public Library of Science, e105050. ISSN: 1932-6203. DOI: 10.1371/journal.pone.0105050.

Ward, D. S. et al. (2012). 'The changing radiative forcing of fires: global model estimates for past, present and future'. In: *Atmospheric Chemistry and Physics* 12.22. Publisher: Copernicus GmbH, pp. 10857–10886. ISSN: 1680-7316. DOI: 10.5194/acp-12-10857-2012.

Watanabe, Hiroshi et al. (2015). 'Global mapping of greenhouse gases retrieved from GOSAT Level 2 products by using a kriging method'. In: *International Journal of Remote Sensing* 36.6, pp. 1509–1528. ISSN: 0143-1161, 1366-5901. DOI: 10.1080/01431161.2015.1011792.

Watkins, Michael M. et al. (2015). 'Improved methods for observing Earth's time variable mass distribution with GRACE using spherical cap mascons'. In: *Journal of Geophysical Research: Solid Earth* 120.4, pp. 2648–2671. ISSN: 2169-9356. DOI: 10.1002/2014JB011547.

Wees, Dave van et al. (2022). 'Global biomass burning fuel consumption and emissions at 500-m spatial resolution based on the Global Fire Emissions Database (GFED)'. In: *Geoscientific Model Development Discussions*. Publisher: Copernicus GmbH, pp. 1–46. ISSN: 1991-959X. DOI: 10.5194/gmd-2022-132.

Werf, G. R. van der et al. (2006). 'Interannual variability in global biomass burning emissions from 1997 to 2004'. In: *Atmospheric Chemistry and Physics* 6.11. Publisher: Copernicus GmbH, pp. 3423–3441. ISSN: 1680-7316. DOI: 10.5194/acp-6-3423-2006.

Wiedinmyer, C. et al. (2011). 'The Fire INventory from NCAR (FINN): a high resolution global model to estimate the emissions from open burning'. In: *Geoscientific Model Development* 4.3. Publisher: Copernicus GmbH, pp. 625–641. ISSN: 1991-959X. DOI: 10.5194/gmd-4-625-2011.

Wiese, David, Felix Landerer and Michael Watkins (2016). 'Quantifying and reducing leakage errors in the JPL RL05M GRACE mascon solution'. In: *Water Resources Research* 52. DOI: 10.1002/2016WR019344.

Wiese, David N. et al. (2019). *JPL GRACE and GRACE-FO Mascon Ocean, Ice, and Hydrology Equivalent Water Height Coastal Resolution Improvement (CRI) Filtered Release 06 Version 02*. Accessed: 2021-09-20. URL: https://podaac.jpl.nasa.gov/dataset/TELLUS_GRAC-GRFO_MASCON_CRI_GRID_RL06_V2.

Wigneron, Jean-Pierre et al. (2021). 'SMOS-IC data record of soil moisture and L-VOD: Historical development, applications and perspectives'. In: *Remote Sensing of Environment* 254, p. 112238. ISSN: 0034-4257. DOI: 10.1016/j.rse.2020.112238.

Withey, Kieran et al. (2018). 'Quantifying immediate carbon emissions from El Niño-mediated wildfires in humid tropical forests'. In: *Philosophical Transactions of the Royal Society B: Biological Sciences* 373.1760. Publisher: Royal Society, p. 20170312. DOI: 10.1098/rstb.2017.0312.

Wooster, M. J., W. Xu and T. Nightingale (2012). 'Sentinel-3 SLSTR active fire detection and FRP product: Pre-launch algorithm development and performance evaluation using MODIS and ASTER datasets'. In: *Remote Sensing of Environment*. The Sentinel Missions - New Opportunities for Science 120, pp. 236–254. ISSN: 0034-4257. DOI: 10.1016/j.rse.2011.09.033.

Worden, John R. et al. (2017). 'Evaluation and attribution of OCO-2 XCO_2 uncertainties'. In: *Atmospheric Measurement Techniques* 10.7. Publisher: Copernicus GmbH, pp. 2759–2771. ISSN: 1867-1381. DOI: 10.5194/amt-10-2759-2017.

Yoshida, Y. et al. (2011). 'Retrieval algorithm for CO_2 and CH_4 column abundances from short-wavelength infrared spectral observations by the Greenhouse gases observing satellite'. In: *Atmospheric Measurement Techniques* 4.4. Publisher: Copernicus GmbH, pp. 717–734. ISSN: 1867-1381. DOI: 10.5194/amt-4-717-2011.

Zammit-Mangion, Andrew, Noel Cressie and Clint Shumack (2018). 'On Statistical Approaches to Generate Level 3 Products from Satellite Remote Sensing Retrievals'. In: *Remote Sensing* 10.2, p. 155. ISSN: 2072-4292. DOI: 10.3390/rs10010155.

Zeng, Z.-C. et al. (2017). 'Global land mapping of satellite-observed CO2 total columns using spatio-temporal geostatistics'. In: *International journal of digital earth* 10.4, p. 426. ISSN: 1753-8947, 1753-8955. DOI: 10.1080/17538947.2016.1156777.

Zheng, Bo et al. (2021). 'Increasing forest fire emissions despite the decline in global burned area'. In: *Science Advances* 7.39, eabh2646. DOI: 10.1126/sciadv.abh2646.

Zscheischler, Jakob et al. (2018). 'Future climate risk from compound events'. In: *Nature Climate Change* 8.6. Number: 6 Publisher: Nature Publishing Group, pp. 469–477. ISSN: 1758-6798. DOI: 10.1038/s41558-018-0156-3.

A Appendix

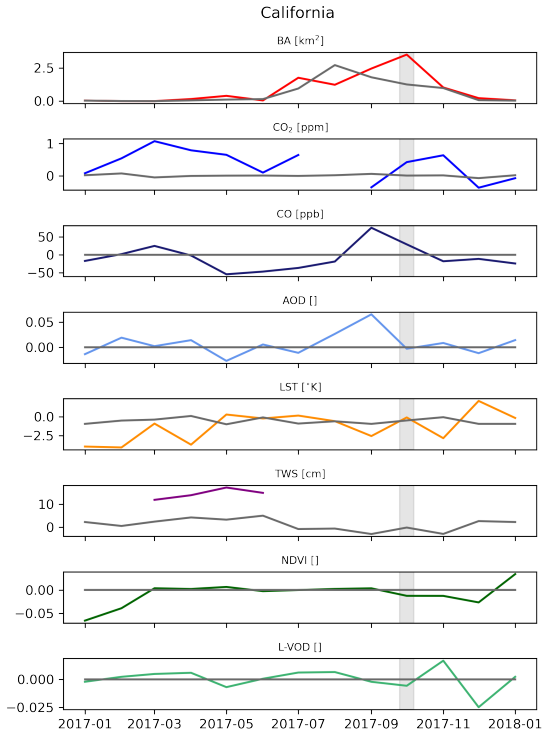

(a)

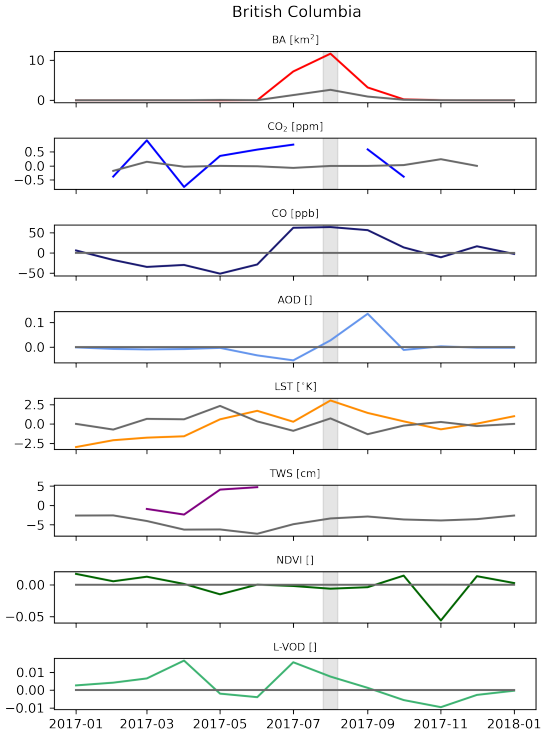

(b)

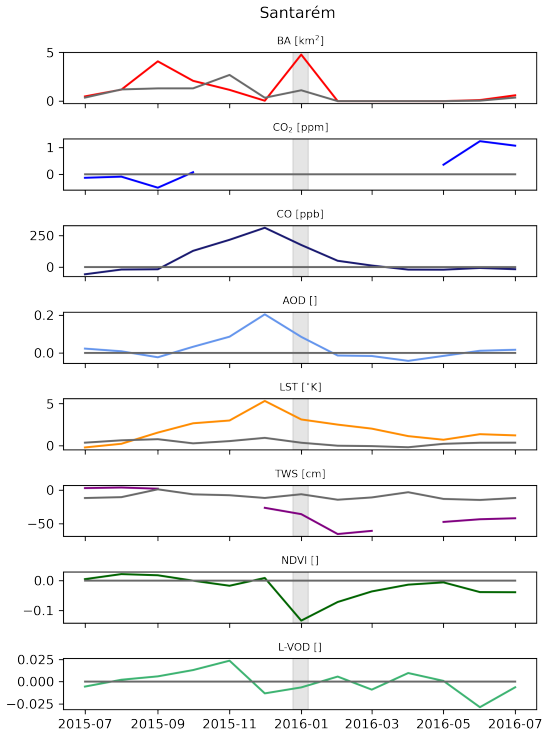

(c)

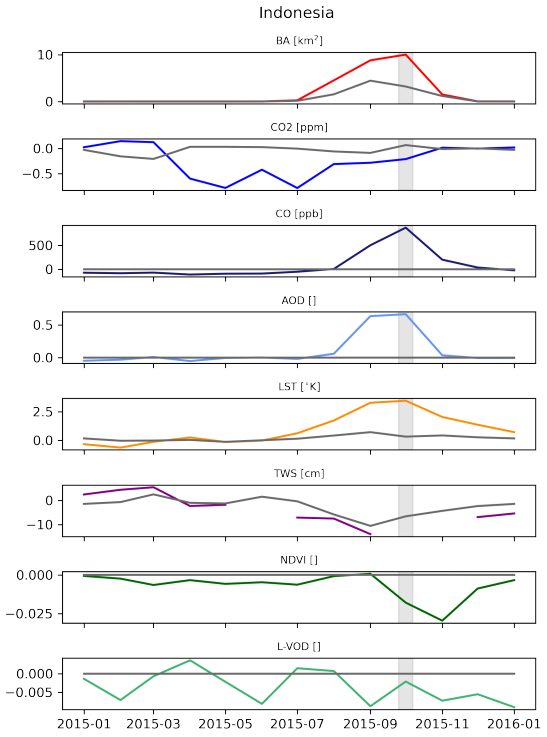

(d)

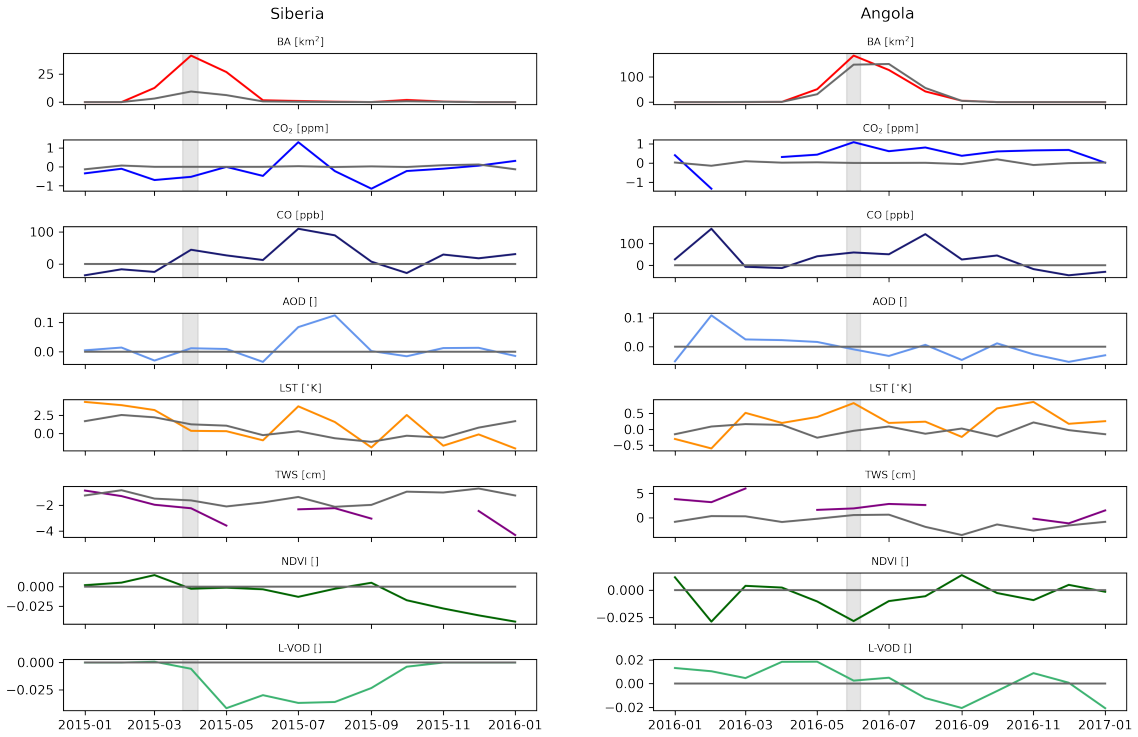

(e) (f)

Figure 12: Time series of BA, carbon, and auxiliary parameters anomalies during an extreme wildfire event in California (12a), and British Columbia (12b), Santarém (Brazil, 12c), Indonesia (12d), Siberia (12e), and Angola (12f). Grey lines indicate the parameters' climatology, based on the period from September 2014 to July 2020. The grey bars mark the month of maximum BA, used here as indicator for the fire peak. Note that the y-axes are not of the same scale.

Declaration of consent

on the basis of Article 30 of the RSL Phil.-nat. 18

Name/First Name: Burger, Martina

Registration Number: 16-050-288

Study program: Climate Sciences

Bachelor ☐ Master ☑ Dissertation ☐

Title of the thesis: Fire Signal Detection in Remote Sensing Carbon Data

Supervisor: Prof. Dr. Olivia Romppainen-Martius

I declare herewith that this thesis is my own work and that I have not used any sources other than those stated. I have indicated the adoption of quotations as well as thoughts taken from other authors as such in the thesis. I am aware that the Senate pursuant to Article 36 paragraph 1 litera r of the University Act of 5 September, 1996 is authorized to revoke the title awarded on the basis of this thesis.

For the purposes of evaluation and verification of compliance with the declaration of originality and the regulations governing plagiarism, I hereby grant the University of Bern the right to process my personal data and to perform the acts of use this requires, in particular, to reproduce the written thesis and to store it permanently in a database, and to use said database, or to make said database available, to enable comparison with future theses submitted by others.

Place/Date

Basel, 09.01.2023

Signature